©2004 by Economic Geology
Vol. 99, pp. 1145–1176

Modeling the Role of Sodic Alteration in the Genesis of Iron Oxide-Copper-Gold Deposits, Eastern Mount Isa Block, Australia

Nicholas H. S. Oliver,† James S. Cleverley, Geordie Mark,* Peter J. Pollard, Bin Fu, Lucas J. Marshall, Michael J. Rubenach, Patrick J. Williams, and Timothy Baker

Predictive Mineral Discovery Cooperative Research Centre and Economic Geology Research Unit, School of Earth Sciences, James Cook University, Townsville, Australia 4811

Abstract

Liberation of iron and potassium by widespread postmetamorphic albitization of country rocks was one of the likely contributing processes in the formation of both barren and mineralized magnetite ± chalcopyrite + biotite + gold + hematite + clinopyroxene + actinolite + apatite ironstones in the Cloncurry district of the Proterozoic Mount Isa block. Whole-rock geochemical data indicate nearly immobile Al, Ga, ±Ti, Zr during transformation of a variety of least altered rocks toward albitite. The data indicate that the addition of Na from a brine to the rock accompanied the loss of Fe, K, Ba, Rb ± Ca, Sr, Co, V, Mn, Pb, and Zn from those altered rocks and enrichment in the brine, but that Cu was not systematically stripped from a variety of wall rocks during albitization. Conversely, the formation of metasomatic ironstones, the immediate hosts to some Cu-Au ores, involves addition of most of the same elements that were lost during albitization. The correlation between intensity of alteration, its distribution and timing (e.g., in breccias cored by ca. 1530–1500 Ma granitoids), and convergence of all rock types toward magmatic stable isotope values provides strong evidence for a substantial component of igneous-derived fluid. Simulations of the albitization process were carried out isothermally at 550°C and 350 MPa and polythermally from these conditions down to 400°C and 200 MPa, using the Gibbs minimization method with HCh software and the UNITHERM database. Both simple fluid-rock mixing models and more complicated reactor-style algorithms used a range of input fluids (from fluids equilibrated fluid with two-feldspar granite through to Na/K ratios consistent with fluid inclusion results) and geochemical data for initially unaltered wall rocks. The apparent paradox of widespread albitization resulting from fluid released by two-feldspar granites can be explained by relatively small shifts away from the K-feldspar-albite equilibrium curve, and even isothermal model fluids derived from two-feldspar granites produce albitites in calc-silicate rocks outboard of granite-proximal K-feldspar-clinopyroxene skarns, matching field patterns. Those models with fluid Na/K ratios similar to those of fluid inclusions produced the most realistic alteration assemblages, dominated by albite, for both isothermal conditions and decreasing temperature, which approximate those observed in the field. PIXE and microthermometric data on fluid inclusions from quartz in two-feldspar quartz monzonite and pegmatite at the top of the Mount Angelay pluton indicate bulk Na/K molar ratios in the fluid of between 10 and 20, considerably higher than our thermodynamically calculated values for fluid in equilibrium with two-feldspar granite of around 3 (at 550°C, 350 MPa). Such shifts may have been attained by admixture of magmatic-hydrothermal fluid with small amounts of NaCl brines trapped along grain boundaries in scapolite-bearing calc-silicate wall rocks, by fluid immiscibility due to high initial CO_2 contents in the felsic intrusions, by contributions from mafic magmas, or from dissolution of salt-rich layers into the intrusions prior to crystallization and fluid release. With increasing amounts of fluid-rock interaction in the models, the fluids were enriched in K, Fe, and Ca, approaching compositions observed in fluid inclusions in the ore deposits. These fluids, reacted with pelitic rocks (which are common ore hosts), would produce magnetite-clinopyroxene ± biotite-actinolite alteration at high temperature, similar to the proximal alteration around ore deposits. We infer that precipitation of sulfides in the Cu-Au deposits was the result of mixing of Cu-bearing brine, of ultimately magmatic origin, but modified extensively via albitization, with sulfur-bearing fluids or reaction of the brine with sulfur-bearing rocks. When Cu was absent from the initial magmatic fluid, barren ironstones may have been the result.

Introduction

The association of sodic (±calcic) alteration with deposits of the mesothermal Fe oxide-Cu-Au category has been recognized for some time (Hitzman et al., 1992; Williams, 1994, 1998; deJong and Williams, 1995; Barton and Johnson, 1996; Frietsch et al., 1997; Haynes, 2000; Marschik et al., 2003), but the role, if any, of the sodic alteration in orebody formation remains uncertain. Alteration of rocks toward albite-rich compositions (albitization) may occur as a consequence of hydrothermal fluid circulation around sea-floor hydrothermal cells (Ito et al., 1983; Bird et al., 1984; Rose et al., 1992) and is thought to occur in the up-temperature portions of such flow systems as a consequence of the thermal dependence of the stability of albite relative to potassic minerals. Albite-rich rocks in continental rifts have also been interpreted as the products of syngenetic, diagenetic, or metamorphic recycling of evaporite components (Cook and Ashley, 1992; Oliver et al., 1994), and Barton and Johnson (1996) proposed that circulation of saline, evaporate-derived brines was instrumental in production of mineralized ironstones in Nevada, stripping iron and base metals from wall rocks during sodic-calcic alteration. (We use "ironstones" here as a general term for

† Corresponding author: e-mail, nick.oliver@jcu.edu.au
* Present address: School of Geosciences, Monash University, Clayton, Australia 3168.

mineralized or barren iron oxide-rich rocks that may or may not have formed by hydrothermal processes). Alternative models, particularly in postmetamorphic environments where basin-derived fluid sources are not readily apparent, appeal to fluid release from igneous crystallization to provide ore-forming constituents in Fe oxide-Cu-Au deposits (Hitzman et al., 1992; Oreskes and Einaudi, 1992). Highly saline fluids may exsolve from crystallizing intermediate or felsic magma and move along down-temperature flow paths (e.g., Cline and Bodnar, 1991), and this has been proposed as the source of metal and brine for La Candelaria (Marschik and Fontboté, 2001; Marschik et al., 2003) and other Andean (Sillitoe, 2003) Fe oxide-Cu-Au deposits and for the postmetamorphic Proterozoic Fe oxide-Cu-Au deposits of the Cloncurry district (Rotherham et al., 1998; Williams, 1998; Mark et al., 2000; Perring et al., 2000; Baker et al., 2001; Pollard, 2001). However, some Fe oxide-C-Au districts, particularly in the lower temperature spectrum, are not associated with regional sodic alteration even when a magmatic source is suggested for some of the ore-forming components (e.g., Skirrow and Walshe, 2002). Important questions for research and exploration for Fe oxide-Cu-Au deposits are (1) were albitizing brines derived from evaporite dissolution or release of fluid from crystallizing magmas or both? (2) if magmatic-hydrothermal fluids were responsible for albitization, how are the high Na/K ratios attained in fluids released by crystallizing two-feldspar granitoids? (3) if evaporite dissolution was responsible for albitization, were evaporites and solvents available, and can a mechanism of interaction with granitoids be found that explains the magmatic stable isotope signatures? (4) is albitization a necessary precursor to Fe oxide-Cu-Au mineralization or is it unrelated? and (5) where were the ore-forming metals and sulfur derived?

Here, we attempt to answer some of these questions by examining regional sodic alteration and mesothermal Fe oxide-Cu-Au deposits of the Eastern Succession of the Mount Isa block (Fig. 1), building on a large number of previous deposit studies, recent regional alteration mapping, stable isotopes, preliminary proton-induced X-ray emission (PIXE) fluid inclusion data, geochronology, and geochemical modeling. In particular, we test the hypothesis of Williams (1994) that at least some ironstones of the Cloncurry district were the products of saline brines whose chemistry was modified through fluid-rock reaction (albitization), and the resulting liberation of Fe, K, and related elements to the fluid. For copper, our geochemical analyses provide some insights as to the likely source(s), and whether or not albitization was crucial for copper enrichment in metasomatic fluids. We also simulate possible reaction paths and mass transfer for fluid-rock interaction using the geochemical modeling package HCh of Shvarov and Bastrakov (1999), which is a Gibbs free energy minimization program particularly suited to high P-T fluid-rock interaction simulations.

Geologic Framework

The Eastern Succession refers to the eastern part of the Mount Isa block, including the Mary Kathleen fold belt in the center, and the Cloncurry district in the east (Fig. 1). Hosts of the alteration and mineralization across the whole Eastern Succession are dominated by calc-silicate rocks, marbles and minor pelitic and volcanic rocks of the 1760 to 1730 Ma Mary Kathleen Group (particularly the Corella Formation), and siliciclastic metasedimentary and mafic metavolcanic rocks of the 1670 to 1620 Ma Soldiers Cap Group. Other rocks include intrusions of various ages, mostly from two main cycles comprising the premetamorphic Wonga Granite and related gabbros (1750–1730 Ma) and the postmetamorphic Williams and Naraku Granites and related gabbros and intermediate intrusions (1550–1500 Ma), referred to here as the Williams Suite. The chronology of deformation, metamorphism, alteration, and mineralization in the Eastern Succession has been explored elsewhere in some depth and is summarized in Table 1. Recently, it has been recognized that the peak metamorphic event, previously inferred to be at ca. 1550 Ma, lies in the range of 1600 to 1580 Ma (Giles and Nutman, 2002; Hand and Rubatto, 2002). The greenschist to upper amphibolite facies "Isan" metamorphism accompanied localized early thrusts and folds (D_1) and widespread upright (D_2) folds. From 1555 to 1500 Ma, there was another major thermal event, associated with intrusion of the Williams Suite, simultaneously with several deformation phases involving ductile shear zones, brittle-ductile fault zones, and brecciation (D_3 and later). Several phases of syn- or post-tectonic intrusions of the Williams Suite can be recognized, including a spatially restricted one at ~1545 Ma (exposed in the southeast) and less well defined but more voluminous phases in the range of 1530 to 1500 Ma (Page and Sun, 1998; Pollard et al., 1998). Widespread albitization (Pollard et al., 1998; Pollard, 2001) and Cu-Au mineralization (e.g., Perkins and Wyborn, 1998; Williams, 1998; Baker et al., 2001) occurred during this period. Notably, however, the Osborne Cu-Au deposit and associated albite alteration record the earlier Isan peak metamorphic cycle, as do several regional albitites in the Snake Creek area (see below). Thermal events and alteration postdating 1500 Ma are not discussed here (see Oliver, 1995).

The characteristics of the Cu-Au deposits have been described in detail elsewhere and are summarized here in Table 2. They generally comprise an association of magnetite, chalcopyrite, pyrite ± pyrrhotite or hematite, surrounded by a proximal (50- to 200-m scale) halo of magnetite ± hematite ± biotite and combinations (at different deposits) of calcite, garnet, chlorite, epidote, diopside, actinolite, orthoamphiboles, K-feldspar, scapolite, titanite, apatite, uraninite, fluorite, and a host of complex phases containing Mn, U, Co, REE, P, and Cl. At the largest deposit, Ernest Henry, conversion of host rocks to magnetite-biotite gangue involved addition of Fe, K, and a range of other elements (Mark et al., 2000). Almost all deposits are surrounded by a distal 100-m to kilometer-scale halo of Na ± Ca alteration, although distinctions between distal and more regional albite alteration are commonly unclear because of the widespread extent of the latter (see below). Fluid inclusions, mostly from quartz veins in the deposits, reveal highly complex brines and CO_2-rich compositions (Table 2), and most of the brines have highly elevated Rb, Ba, K, Ca, Fe, Mn, Cu, Pb, and Zn concentrations (Williams et al., 1999, 2001; Mark et al., 2000; Perring et al., 2000). Stable isotope data for carbonates and sulfides are dominated by apparent igneous signatures, with local influences of host-rock carbon and sulfur (Davidson and Dixon, 1992; Mark et al., 2000). However, the deposits are mostly distal to intrusions, with

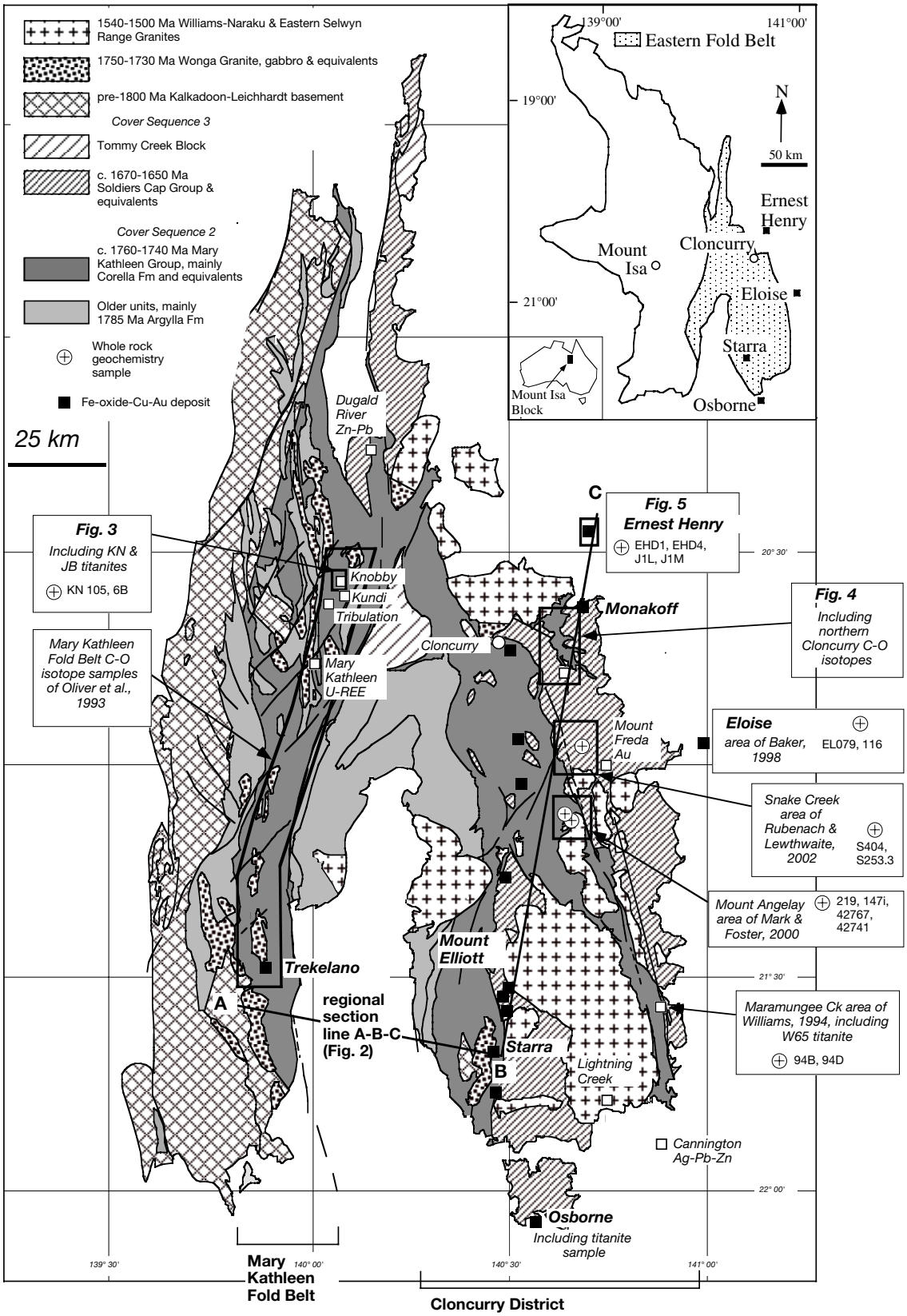

FIG. 1. Map of the Eastern Succession of the Proterozoic Mount Isa block, showing the location of more detailed maps and cross sections in this paper and locations of study areas from previous papers, the major Fe oxide-Cu-Au deposits, other localities mentioned in the text, and whole-rock geochemistry and titanite geochronology locations. Inset shows the location of the Eastern Succession of the Mount Isa block in northern Australia. Modified from Williams (1998).

TABLE 1. General Characteristics and Interpreted Fluid Sources of Regional Alteration (1750–1500 Ma) in the Eastern Mount Isa Block

Event	Mineral associations	Extent, host rock	T-P	General references	Fluid source, references
Wongan extension and intrusions (1750–1730 Ma)					
Skarns Shear zones Dolerite alteration	Cpx-gt-sc skarns Sc-ab shear zones Sc-am alteration in mafic rocks	Km scale in calc-silicate rocks M to 100-m scales in granite 100-m to km scales in dolerites	500°–700°C, 150 –200 MPa	Oliver et al. (1994), Oliver (1995)	Metamorphic, evaporitic, magmatic (Oliver et al., 1994)
Regional metamorphism (1600–1580 Ma, Isan orogeny)					
Regional metamorphism of calc-silicate and pelitic rocks	Sc-qz-cc-kf ± bt-am-cpx-ttn-ap-mt-ilm in calc-silicate rocks, bt-mu-qz ± and-crd-ky-st-gt-ilm in pelites	District scale, variably preserved at mm to km scales in metasediments	500°–670°C, 300–450 MPa	Oliver et al. (1991, 2001), Laing (1998), Giles and Nutman (2002), Hand and Rubatto (2002)	Metamorphic-evaporitic (locally derived, Oliver et al., 1992)
Albite shear zones and patches	Ab-ru ± qz-bt-kf-crd-st-ged in pelites	100-m to km scale in pelites, mostly Snake Ck and Osborne mine surrounds	500°–690°C, 300–450 MPa	Rubenach and Barker (1998)	Magmatic/metamorphic? + evaporite (Rubenach and Lewthwaite, 2002)
Osborne Cu-Au deposit	Mt-bt-qz-ab-cpy-py-po ± am-cc-mu-ht	100-m scale in BIF?, feldspathic metapelites and arenites	500°–650°C, 300–400 MPa	Gauthier et al. (2001) Rubenach et al. (2001)	Magmatic? + evaporite (R. Mustard, pers. commun., 2003)
Thermal metamorphism (1550–1500 Ma, Williams batholith)					
Early Williams batholith 1550–1520 Ma	Zoned pegmatite-ab-qz-am-ap veins, UST	Plutons and roof pendants, e.g., Mt. Angelay Granite	500°–650°C, 300–400 MPa	Page and Sun (1998), Pollard et al. (1998), Mark et al. (1999), Davis et al. (2001)	Magmatic (Mark et al, 1999; Mark and Foster, 2000; Pollard, 2001)
Later Williams batholith 1530–1500 Ma	Mairolitic cavities with qz-cc, qz-ab ± am-mt-py breccia	Plutons and widespread stocks and polymictic breccia cutting pelitic and calc-silicate rocks	500°–700°C, 200–300 MPa	Page and Sun (1998), Pollard et al. (1998), Mark et al. (1999), Davis et al. (2001)	Magmatic (Mark et al, 1999; Mark and Foster, 2000; Pollard, 2001)
Lightning Ck prospect	Mt-ap-ttn ironstones	100-m scale, intrusion hosted	500°–700°C, 200–400 MPa	Perring et al. (2000)	Magmatic (Perring et al., 2000; Pollard, 2001)
Albitites	Ab-am-ttn ± cpx-ep-ap-cc in calc-silicate rocks; ab-ru-bt ± act-ged-crd in pelites; ab-am-ttn ± cpx-sc and am ± cc veins in mafic rocks	Regional, abundant in all rock types, shear zones, veins, and alteration, breccias	450°–600°C, 200–400 MPa	Oliver et al. (1990, 2001), Oliver (1995), deJong and Williams (1995), Baker and Laing (1998), Laing (1998), Mark (1998a)	Modified magmatic? (Oliver et al., 1993; this study)
Barren ironstones	BIF?, metasomatic replacement, veins	Local to abundant in pelitic, calc-silicate and mafic rocks	No constraints	Williams (1998)	Modified magmatic? (this study)
Fe oxide-Cu-Au deposits	Mt-cpy-py-ap-ttn-bt-Au ± cc-po-ht-sc-am-gt-flu-bar	Felsic volcanic, politic, and mafic rock hosts	370°–470°C, 150–400 MPa	Summary in Williams (1998), Baker (1998), Rotherham et al. (1998), Mark et al. (2000), Baker et al. (2001), Williams et al. (2001)	Modified magmatic? (Mark et al. 2000; Baker et al., 2001)

Abbreviations: ab = albite, ap = apatite, am = actinolitic to complex calcic amphibole, and = andalusite, bar = barite, bt = biotite, cc = calcite, cpx = clinopyroxene, cpy = chalcopyrite, crd = cordierite, ep = epidote, flu = fluorite, ged = gedrite, gt = garnet (grossular-andradite in skarns, almandine-spessartine in pelites), ht = hematite, ilm = ilmenite, ky = kyanite, mt = magnetite, mu = muscovite, po = pyrrhotite, py = pyrite, qz = quartz, sc = scapolite (mostly sodic), st = staurolite, ttn = titanite, UST = unidirectional solidification texture

TABLE 2. Characteristics of Major Iron Oxide-Cu-Au Deposits of the Eastern Mount Isa Block

Deposit, size, grade, references	Age and T-P estimates	Host rocks and structure	Ore and alteration mineralogy and element associations	Fluid inclusion chemistry	S, C, O isotopes (‰)
Ernest Henry, 167 Mt at 1.1% Cu, 0.54 g/t Au (Twyerould, 1997; Mark et al., 1999, 2000)	≥1514–1504 Ma Ar-Ar bt, 450°C (F.I. and O isotopes), 150–370 MPa (CO_2 F.I. density)	Mary Kathleen Gp. (Corella Fm.?) K-feldspar–altered intermediate volcanic rocks, brecccia sheet in bend in brittle-ductile shear zone	Cpy, py, mt, cc ore in mt, bt, kf, gt, py, ht, bar, mu; Fe, Mn, Mo, As, Co, K, Ba, F, U, Ag	(A) hypersaline L-V halite ± 5 other daughters, 33–55 wt % NaCl equiv (B) moderate salinity L-V ± halite, ca. 20 wt % NaCl equiv (C) CO_2 rich	$\delta^{34}S_{py}$ = –2 to +4, $\delta^{34}S_{cpy}$ = –1 to +4, $\delta^{13}C_{cc}$ = –6 to 0, $\delta^{18}O_{cc}$ = 10 to 13
Osborne, 15.2 Mt at 3.0% Cu, 1.05 g/t Au (Adshead et al., 1998; Rubenach et al., 2001; Gauthier et al., 2001)	1600–1590 Ma (Re-Os molybdenite and U-Pb titanite), 1570–1540 Ma (Ar-Ar hb and bt), >450°C and 150 MPa	Soldiers Cap Gp. feldspathic to pelitic schist, amphibolite and ironstone; bend or fold in ductile shear zone	Cpy, py ± ht or po ore in mt, bt, qz, ab, hb, mu, cc in ironstone; Fe, Co, Bi, W, Se, Hg, Te, Cl, Sn, Mo, P, B	(A) hypersaline L-V halite ± 4 other daughters, <70 wt % NaCl equiv (B) CO_2-CH_4	$\delta^{34}S_{py}$ = –2 to +6, $\delta^{34}S_{cpy}$ = –6 to +2, $\delta^{13}C_{cc}$ = –7 (1 sample) $\delta^{18}O_{cc}$ = 15 (1 sample)
Starra, 7.4 Mt at 1.9% Cu, 3.8 g/t Au (Rotherham et al., 1998; Williams et al., 2001)	>1505 Ma (Ar-Ar bt), 400°–550°C early, 220°–360° late, > 130 MPa (F.I.)	Mary Kathleen Gp. bt-rich schists and ironstones; ductile shear zone and related breccciation	Cpy, py, ht ore and related cc, anh ± bar veins in mt, bt-chl, ht, ab in ironstone; Fe, Co, W, Sn, F, Mo, Y, REE	(A) hypersaline L-V halite ± 3 other daughters including mt, 34–52 wt % NaCl equiv (B) hypersaline L-V halite ± 4 other daughters, Ba-Mn rich, 29–42 wt % NaCl equiv (C) CO_2 rich	$\delta^{34}S_{py}$ = –5 (1 sample) $\delta^{34}S_{cpy}$ = –6 to –3 (2 samples), (3 outliers –10 to –5) $\delta^{13}C_{cc}$ = –7 to –1, $\delta^{18}O_{cc}$ = 10 to 13
Eloise, 3.1 Mt at 5.5% Cu, 1.4 g/t Au (Baker, 1998; Baker et al., 2001)	1530 Ma (Ar-Ar hb), 430°–550°C qz-hb O isotopes, ca. 450°C F.I.	Soldiers Cap Gp. psammite, pelite, amphibolite; veins in brittle-ductile shear zone	Po, cpy, py ore in hb, bt, mt, py, cc, qz, act, chl; Ag, Co, Ni, As, Bi	(A) hypersaline L-V halite ± 4 other daughters, 30–68 wt % NaCl equiv (B) CO_2 rich, late	$\delta^{34}S_{py}$ = 0 to 2, $\delta^{34}S_{cpy}$ = 1 to 2, $\delta^{13}C_{cc}$ = –10 to –8, $\delta^{18}O_{cc}$ = 9 to 10
Mt. Elliott, 3.3 Mt at 3.6% Cu, 1.8 g/t Au (Little, 1997)	>1505 Ma (Ar-Ar bt), 350°–500°C	Soldiers Cap Gp. graphitic schist and amphibolite; brecciated dilatant jog in sheared skarn	Py, po, cpy ore in mt, cpx, sc, ab; F, P, Co, Ni, LREE, Mo	(A) hypersaline L-V halite ± 4 other daughters (C) CO_2 rich	$\delta^{34}S_{py}$ = 0 to 2, $\delta^{34}S_{cpy}$ = 1 to 2, $\delta^{13}C_{cc}$ = –10 to –8, $\delta^{18}O_{cc}$ = 12 to 13

Deposit locations are shown in Figure 1; see also Williams (1998); abbreviations as for Table 1 but also act = actinolite, anh = anhydrite, chl = chlorite, F.I. = fluid inclusions, hb = hornblende, kf = K-feldspar

only the Mount Elliott deposit lying within 1 km of an exposed kilometer-scale intrusion (Fig. 1). Ore deposition is thought to have occurred by two main mechanisms: reaction of Cu-bearing brines with previous ironstones and/or sulfide-bearing rocks such as black shales (Davidson and Dixon, 1992; Williams, 1998; Baker et al., 2001), or reaction of two (or more) fluids, including one or more Cu-bearing brines, and an S-bearing fluid of varying oxidation state (e.g., Mark et al., 2000; Williams et al., 2001).

Distribution, Nature, and Timing of Albitite

In the Eastern Succession, there are several major phases of alteration and mineralization spanning more than 250 m.y. (Table 1). Oliver et al. (1994) recognized synextensional (ca. 1740 Ma) sodic-calcic alteration in the Mary Kathleen fold belt in the westernmost part of the Eastern Succession, which shares several features with the sodic alteration in the Humboldt Lopolith district in Nevada (Vanko and Bishop, 1982; Barton and Johnson, 1996). In both areas, voluminous mafic (±felsic) intrusions emplaced into sedimentary sequences containing abundant evaporites were interpreted to have resulted in circulation of saline brines and production of sodic scapolite (dominant over sodic plagioclase), synchronous or slightly predating development of calcic, scapolite-bearing skarns proximal to granitoids. In the Mary Kathleen fold belt, the altered rocks are readily identified by their preservation in distinctive 1- to 10-km-scale lozenges preserving early intrusive, metasomatic, and contact metamorphic relationships,

surrounded by regionally metamorphosed rocks that wrap around the altered rocks due to strain partitioning (Oliver, 1995). The altered rocks are relatively restricted in extent, predate deposition of the Soldiers Cap Group that elsewhere is mineralized, and are not discussed further here.

During the 1600 to 1580 Ma Isan orogeny, some foliated rocks developed abundant albite, particularly in Soldiers Cap Group pelites at the Osborne mine and in the Snake Creek area (Adshead et al., 1998; Rubenach and Barker, 1998; Rubenach et al., 2001; Rubenach and Lewthwaite, 2002). No major intrusions appear to have been temporally associated with this alteration, although pegmatites are abundant at Osborne. The rocks reached maximum P and T of 450 MPa and ≥650°C, determined by pelite mineral equilibria and thermobarometry (Rubenach and Lewthwaite, 2002). Albitization occurred relatively early in this cycle, at approximately 500° to 550°C and ≤400 MPa; the specific timing and P-T conditions of the albitization are tightly constrained by relationships between biotite, albite, and orthoamphiboles in and around andalusite porphyroblasts and by the absence of paragonite (Rubenach and Lewthwaite, 2002). These rocks are distributed in broad, foliation parallel alteration zones surrounding centimeter- to meter-scale zones of intense albitization and are transgressive to bedding at meter to 100-m scales (Table 3). At millimeter to centimeter scales, the transition into albitized rocks is marked by replacement of matrix quartz and muscovite by albite and rutile, with localized development of orthoamphibole and cordierite; biotite is also consumed in the most altered rocks. These rocks, described in detail by Rubenach and Lewthwaite (2002), are used for some of the modeling presented below.

The third type of alteration and the focus of this paper includes widespread and layer-transgressive albite (Table 3).The clearest evidence for the relative timing of most of the

TABLE 3. Associations of Albitites during the Isan Orogeny and Williams Thermal Event

Association	Timing, T-P conditions, references	Host rocks	Prealteration (or primary) assemblages	Alteration/vein assemblages, (% of area affected)	Fluid chemistry
Isan orogeny (1600–1580 Ma)					
100-m- to km-scale high-strain zones parallel to major D_2 fold axial zones	1600–1580 Ma, 500–650°C, 300–450 MPa (Foster and Rubenach, 2000; Gauthier et al., 2001; Rubenach and Lewthwaite, 2002)	Pelitic rocks of Soldiers Cap Gp., Snake Creek, and Osborne	Mu, bt, qz, ilm ± and, gt, sill, kf, ky, st	Ab, ru ± oam, crd, mt, bt, qtz, chl; rare act, mt, cpx (5%)	No F.I., chemical modeling, this study
Williams thermal event (1550–1500 Ma)					
(1) 10-m- to 100-m-scale D_3 high-strain zones along rock contacts	1555–1540? Ma, 400°–600°C, 300–400 MPa (Oliver, 1995; Mark et al., 2000, 2001)	Calc-silicate rocks of Mary Kathleen Gp., amphibolitic metadolerites, metatonalites	Sc-bt-qz-cc ± am-cpx-ep-kf-ttn-ap in calc-silicate rocks, am-pl-ttn-ilm ± sc-cpx-to in metadolerites	Ab-ttn ± am-cpx-bt-ap-ep-mt-ht-py (5%)	F.I. from associated veins (see below); $\delta^{34}S_{py}$ = –1 to +1‰ at Ernest Henry; C, O isotopes see Fig. 12
(2) Cm- to 100-m-scale veins	1555–1500 Ma, 475°–600°C, 300–450 MPa (Oliver et al., 1993; Oliver, 1995; Mark, 1998a)	Calc-silicate rocks of Mary Kathleen Gp., amphibolitic metadolerites, metatonalites	Sc-bt-qz-cc ± am-cpx-ep-kf-ttn-ap in calc-silicate rocks, am-pl-ttn-ilm ± sc-cpx-to in metadolerites	(A) cc-qz-am-cpx ± ab-dol-py-cpy-ap-bt (B) am ± cpx-mt-py-ab-cc (5%)	C, O isotopes see Fig. 12. F.I. (Fu et al., 2003) (1) variable density CO_2, 200–400 MPa; (2) L + V ± halite, Ca-bearing; (3) multisolid hypersaline halite-sylvite ± cc-mt
(3) Layer-transgressive alteration around (2) veins	1555–1500 Ma, 475°–600°C, 300–450 MPa (Oliver et al., 1993; deJong and Williams, 1995; Oliver, 1995; Mark et al., 2001)	Calc-silicate rocks of Mary Kathleen Gp., amphibolitic metadolerites, metatonalites	Sc-bt-qz-cc ± am-cpx-ep-kf-ttn-ap in calc-silicate rocks, am-pl-ttn-ilm ± sc-cpx-to in metadolerites	Ab-ttn ± am-cpx-bt-ap-ep-mt-ht (10%)	Association with (2) veins; C, O isotopes see Fig. 12
(4) 10-m- to km-scale breccias along faults and around granite stocks	1535–1500 Ma based on intrusion ages and titanites; 475°–600°C, 300–450 MPa (Mark, 1998b; Mark and Foster, 2000; Mark et al., 2001; this study)	Calc-silicate rocks, pelites, dolerites, gabbros, diorites	As for rock descriptions above	As for (3) in calc-silicate and mafic rocks; ab-ru ± bt-ttn-act-oam-qtz-crd-mt (10–20% in Mary Kathleen fold belt; up to 50% in Cloncurry)	C, O isotopes see Fig. 12; F.I. (Fu et al., 2003; this study); (1) rare high density CO_2, (2) multi solid hypersaline halite-sylvite ± cc-mt-cpx, (3) halite-H_2O-$CaCl_2$

Abbreviations as for Table 2 but also oam = orthoamphibole, pl = intermediate to calcic plagioclase, ru = rutile, to = tourmaline

albitization comes from an association of albite-rich alteration zones with shear zones, veins, and breccia that cut the regional ductile structural fabrics (see also Oliver et al., 1990; Williams, 1994; deJong and Williams, 1995; Oliver, 1995; Baker and Laing, 1998; Laing, 1998; Mark, 1998a, b). Albitization during this stage reached temperatures of 450° to 600°C, determined from concurrently developed calc-silicate mineral equilibria and calcite-dolomite geothermometry on related veins (Oliver et al., 1993; Oliver, 1995), and oxygen isotope geothermometry on quartz, magnetite, albite, and amphibole (Mark, 1998a; Mark and Foster, 2000). Pressures are not well constrained by mineral geobarometers, but conventional microthermobarometry on high-density CO_2-rich fluid inclusions in quartz vein material associated with albitites indicates entrapment at 200 to 450 MPa at assumed temperatures of 400° to 600°C (Mark et al., 2000; B. Fu et al., unpub. data).

At 100-m to kilometer scales, albite alteration is distributed along broader zones of contrasting rheology in the Mary Kathleen fold belt (Oliver et al., 1990; Figs. 2–3) and in isolated kilometer-scale breccia bodies (e.g., Mount Philp Breccia). In the Mary Kathleen fold belt, approximately 20 percent of the exposed rocks are affected by intense zones of veining and related albitization (Fig. 3, Table 3). In the Cloncurry district, albite alteration and brecciation is very widespread in the Corella Formation and other Mary Kathleen Group equivalents but is moderately restricted in the pelitic rocks. At least some of the localization at this scale appears to be dependent on an association with small stocks and roof zones of the Williams batholith, and with faults (Figs. 2, 4).

At meter to 100-m scales, albite-altered rocks of the same timing are found in every rock type within the Easterm Succession (Figs. 4–6, Table 3), although to a lesser extent in the Williams batholith granitoids (Mark, 1998a; Pollard, 2001). It occurs in meter-scale shear zones (Figs. 6a, 7a), around veins dominated by calcite or actinolite (Figs. 6–7b, c), and in very widespread brecciated rocks (Figs. 4–6, 7d). Albite alteration is predominantly discordant to bedding in metasedimentary rocks, the most obvious controls at this scale being relationship to zones of dilation or shear developed during the D_3 deformation event. These zones of dilation are best developed along the contacts between rocks of contrasting rheology and along fault zones, as explored in depth by Oliver et al. (1990) and Marshall and Oliver (2002). Both the Fe oxide-Cu-Au mineralization and the albite alteration share similar structural controls, commonly being best developed in brittle-ductile shear zones in which synshearing albitization predated or was synchronous with ore-related alteration. Around the Ernest Henry deposit, for example (Fig. 5), albite-rich Na ± Ca alteration lies along lithologic contacts but also within the rock masses, particularly around faults and brittle-ductile shear zones. In detail, it has an almost antithetic relationship with the distribution of ore-related potassic alteration assemblages but is also locally overprinted by the latter, as shown in Figure 5.

Pegmatites occur locally within or crosscutting some albite breccia bodies. At the Tribulation Quarry (Marshall, 2003;

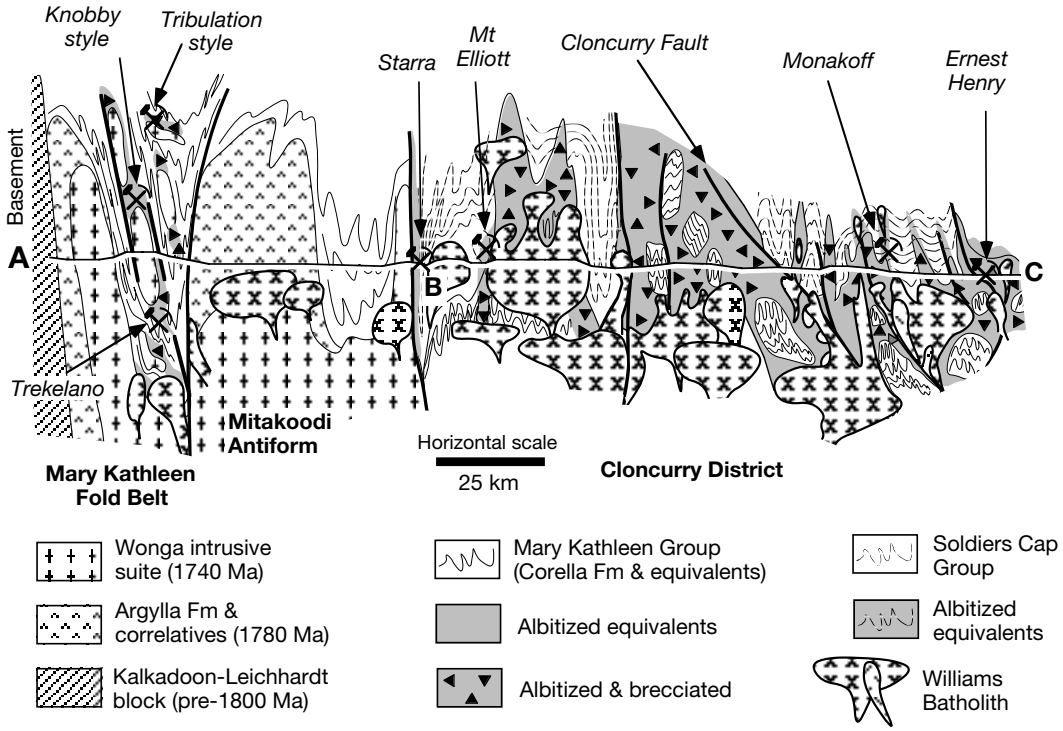

FIG. 2. Schematic cross section of the Eastern Succession of the Mount Isa block, showing the general distribution of major rock units, alteration, brecciation, faults, and Cu-Au mineral deposits, corresponding to the section line A-B-C in Figure 1. Williams-age intrusions below the Mary Kathleen fold belt are inferred; the positions of the other intrusions are extrapolated from the map but depths and detailed shapes are uncertain. The vertical scale is exaggerated, approximately 10:1 to 20:1.

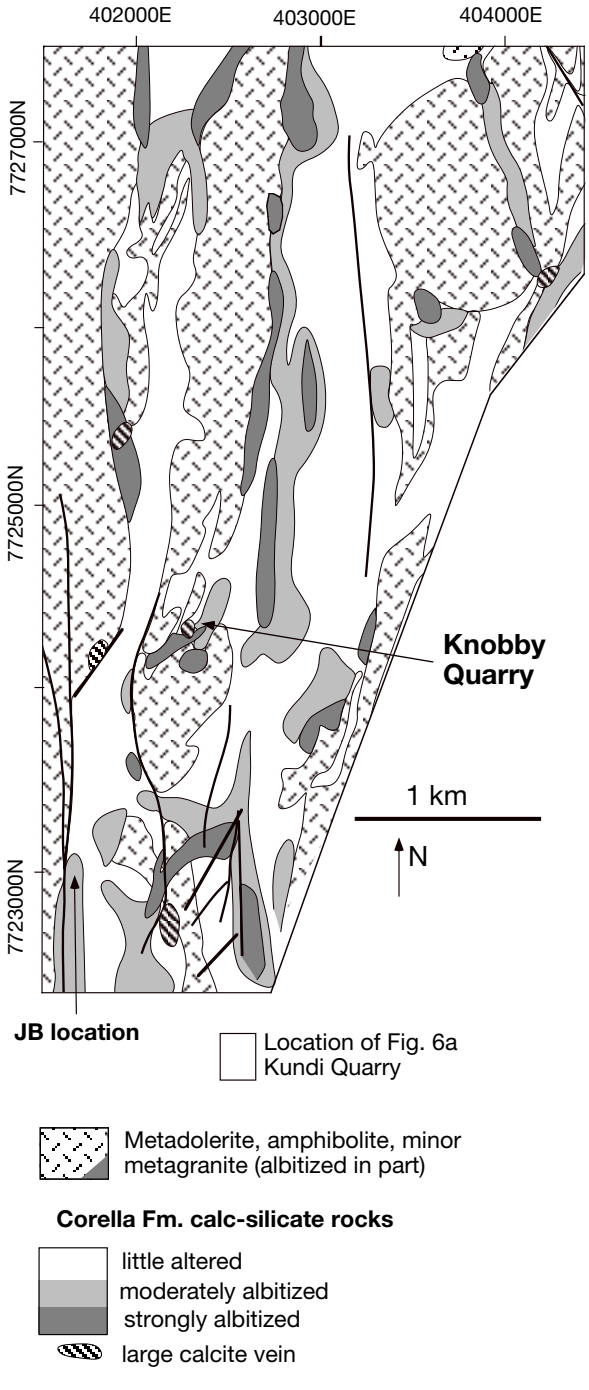

FIG. 3. Details of mapped albite alteration and calcite veins in part of the Mary Kathleen fold belt, adapted from Oliver et al. (1990). Australian map grid coordinates are indicated. For location see Figure 1. Locations of titanite samples from the Knobby Quarry and JB locality are indicated. Little altered = <5 percent of meter- to 10-m-scale outcrops containing any albite or related calcite veins, moderately albitized = 20 to 80 percent of meter- to 10-m-scale outcrops containing ca. 30 to 90 percent albite (including related calcite veins and other calc-silicate alteration minerals), strongly albitized = 70 to 100 percent of meter- to 10-m-scale outcrops containing 70 to 100 percent albite (including related calcite veins and other calc-silicate alteration minerals). Note that alteration occurs mainly on rock contacts, as a consequence of stress and strain heterogeneities developed during deformation (Oliver et al., 1990). The remainder of the Mary Kathleen fold belt shows similar patterns. The location of Figure 6a lies 300 m south of the bottom of Figure 3, as indicated.

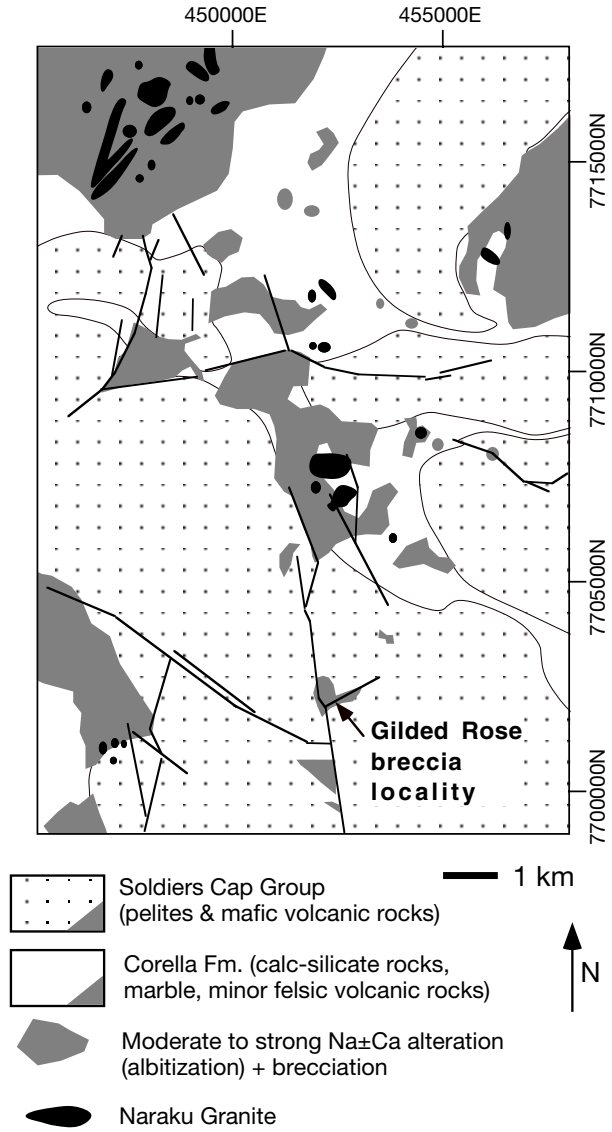

FIG. 4. Map of the broad distribution of albite alteration and brecciation in the northern Cloncurry district, adapted from Marshall (2003). For the altered zones, at meter to 10-m scales, 20 to 100 percent of the rocks contain in excess of 10 percent albite, and details of the intensities of alteration are similar to those depicted for altered zones in Figure 3. For location see Figure 1. Australian map grid coordinates are indicated. The remainder of the Cloncurry district shows a similar or greater extent of albitization. Note the widespread alteration in the Corella Formation but restriction of alteration to the vicinity of faults in the overlying Soldiers Cap Group. Abundant minor intrusions of the Naraku batholith occur at the core of many of the altered zones.

Fig. 1), pegmatite both cuts albite breccia and is contained as clasts within breccia, confirming that periods of intrusion and albitization overlapped. Postbrecciation pegmatite sheets, themselves albitized, are found at Knobby Quarry (Fig. 6b). In the Snake Creek and Gilded Rose regions near Cloncurry, albite breccias are commonly cored by meter- to 10-m-scale pegmatites (Fig. 4). Mark (1998a, b), Pollard et al. (1998), Mark and Foster (2000), Perring et al. (2000), and Pollard (2001) have described direct relationships between roof pendants of the Williams batholith intrusions and local

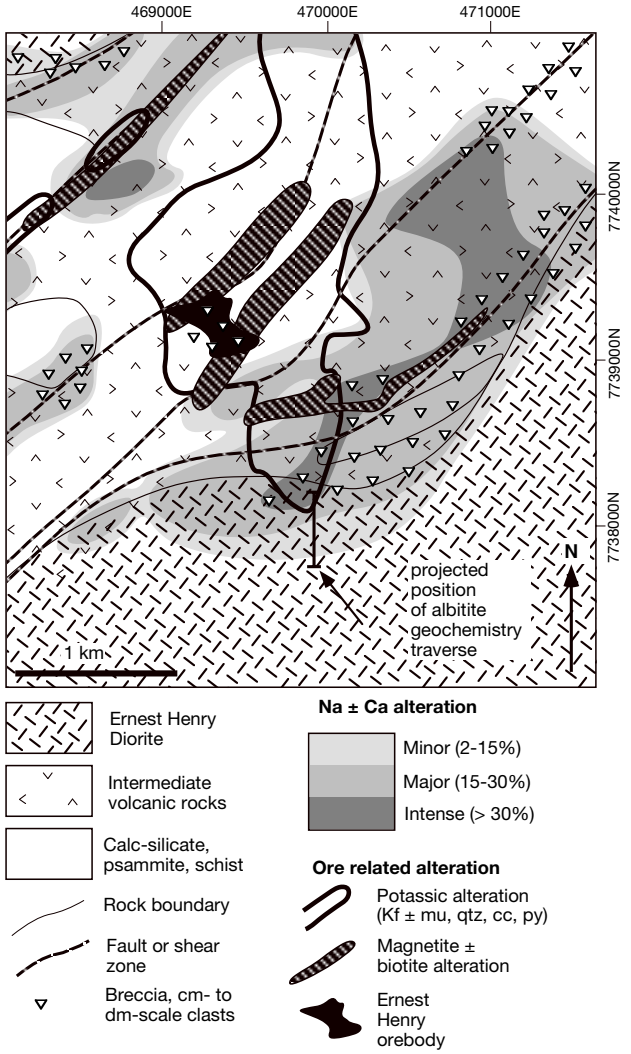

FIG. 5. Map of the detailed distribution of two of the major phases of alteration and mineralization around the Ernest Henry Cu-Au deposit, based on logging of 110 diamond drill holes (Mark et al., 2000), the resource model for the deposit, and the location of major aeromagnetic highs (aeromagnetic data courtesy Ernest Henry Mining). Drill hole data are projected to the 1947 relative level but aeromagnetic highs are projected to the surface. For location see Figure 1. Australian map grid coordinates are indicated. Na ± Ca alteration: minor = 5 to 15 percent of meter-scale drill core intervals containing rocks with ca. 80 to 100 percent albite, major = 15 to 30 percent of meter-scale drill core intervals containing rocks with ca. 80 to 100 percent albite, intense = 30 to 100 percent of meter-scale drill core intervals containing rocks with ca. 80 to 100 percent albite. Altered zones contain additional alteration minerals and veinlets, so these descriptions of major and intense alteration are similar to the moderately and strongly albitized zones depicted in Figure 3. Potassic and magnetite-biotite alteration zones are not subdivided due to their complexity but typically contain >50 percent total of the indicated minerals in meter-scale drill core intervals. The Ernest Henry orebody is dominated by magnetite, pyrite, chalcopyrite, and calcite. Na-Ca alteration is mostly distributed along rock boundaries and shear zones; the orebody and proximal ironstones also lie in brecciated zones between shear zones but the ore-related K-Fe alteration is somewhat discordant.

albitization and proposed that fluids released during magma crystallization were largely responsible for the albitization. At Mount Angelay, Mark (1998a, b) described a complex magmatic-hydrothermal transition (e.g., Fig. 7d) with unidirectional solidification textures in pegmatites grading laterally into hydrothermal infill, the latter including albite and actinolite. In the country rocks surrounding this pluton (and others in the district), calc-silicate rocks locally form proximal clinopyroxene-K-feldspar-albite ± actinolite-garnet skarns up to 20 m from the contacts. More common, however, are broad zones of albitization extending away from the intrusion, in which albite and actinolite compositions are very similar to those developed in the quartz monzonite roof pendants (Mark, 1998a). Geochemical models relating to this situation are presented below.

At millimeter to centimeter scales, fine-grained mosaics of albite replaced feldspars, scapolite, and quartz (Fig. 7e, f). Locally, granoblastic, polygonal calcite and scapolite that formed in calc-silicate rocks during regional metamorphism (Fig. 7e) were replaced by albite and a second generation of coarser grained calcite. Clinopyroxene and titanite ± actinolite formed in calc-silicate and mafic rocks during albitization, replacing earlier biotite and pargasitic to hastingsitic amphiboles. In pelites, albite and rutile replaced micas and quartz, but actinolite formed rarely, particularly near contacts with granites and/or calc-silicate rocks. Albitization commonly involved the production of titanite from the breakdown of biotite ± Fe-Ti oxides via the forward progress of (unbalanced) reactions such as (1) biotite + plagioclase ± K-feldspar ± magnetite ± ilmenite + NaCl ± $CaCl_2$ ± CO_2 → albite + titanite ± scapolite ± calcite + KCl (e.g., in intrusive rocks); (2) biotite + calcite + quartz + NaCl → actinolite + albite + titanite + KCl + CO_2 ± microcline (in impure marbles); and (3) muscovite + biotite + plagioclase (or calcite) + NaCl → tremolite/actinolite + albite + titanite + KCl (in weakly calcareous metapelites). Unequivocal evidence for the production of titanite via these reactions has been gathered from localized zones where the host rock is transitional to the titanite-bearing metasomatic product over centimeter scales (Fig. 7e, f and traverse in Fig. 6b), particularly in narrow metasomatized shear zones, around pegmatites, in reaction zones surrounding veins or related breccia matrix, and uncommonly at the edges of the veins themselves. These relationships allow precise determination of albite alteration paragenesis.

Titanite U-Pb geochronology

If titanite is precipitated during subsolidus metasomatic reactions, then it can be used to date the alteration, provided the rock did not subsequently exceed the 650° to 700°C blocking temperature (Scott and St-Onge, 1995; Pidgeon et al., 1996; Frost et al., 2000). Metasomatic titanite formed predominantly at 400° to 600°C, as in the Eastern Succession of the Mount Isa block, should fulfill this criterion because the post-1500 Ma history of the block involved little thermal disturbance. Small titanite grains (<5 mm) from albite-altered wall rocks were separated at James Cook University by hand crushing the sample material to <500 μm. After washing and cleaning, inclusion-free, translucent to transparent, titanite grains were picked by hand for thermal ionization mass spectrometry (TIMS) analysis. At the Curtin University TIMS facility and laboratory, air abrasion was used on some titanite grains to remove the potentially altered surface layer, which helps to obtain more concordant results. Grains were cleaned, dissolved, and spiked following the procedure of Pidgeon et al. (1996). Isotopic analyses were made on the

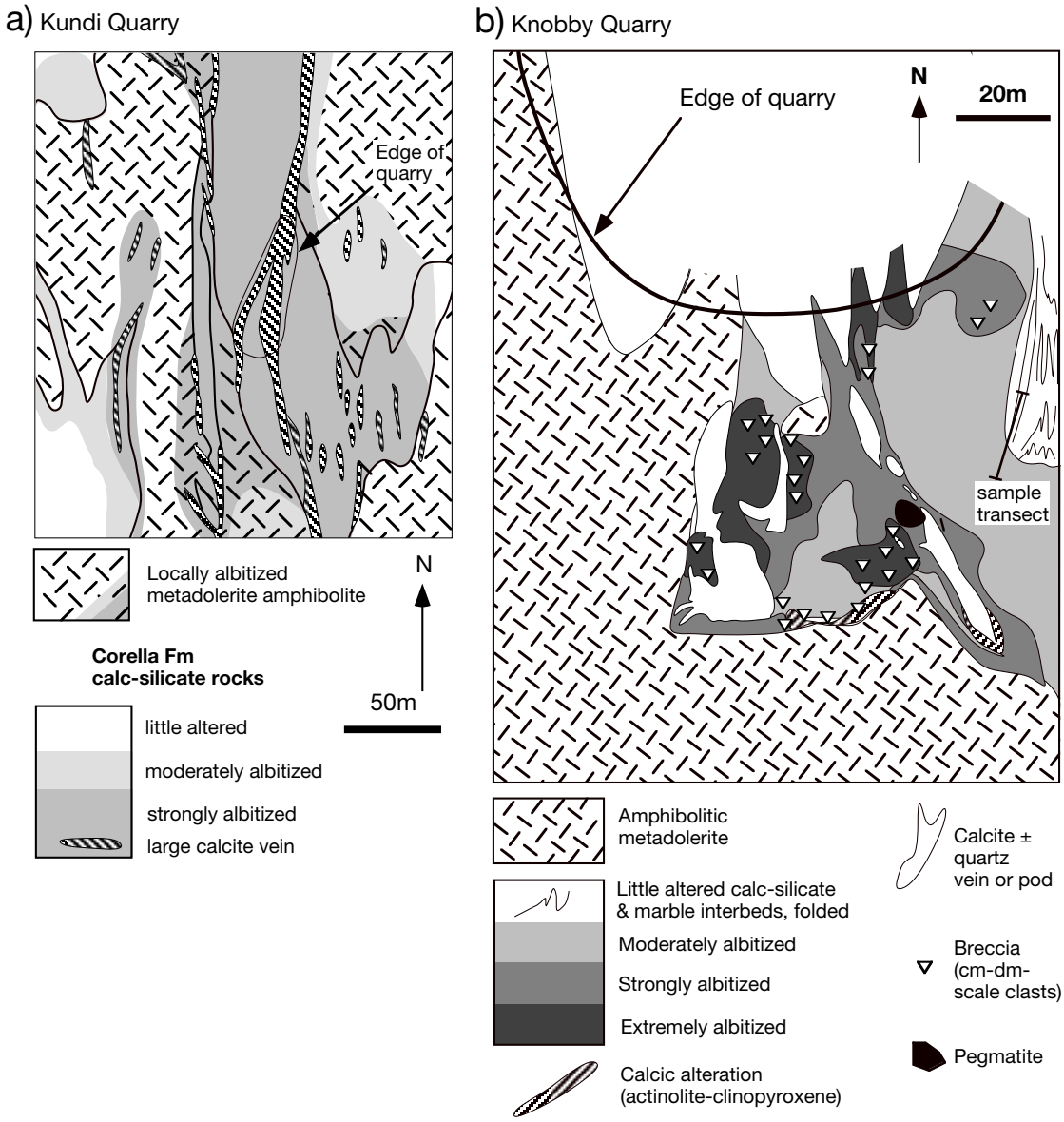

FIG. 6. Detailed maps of albitization and related calcite veining at the (a) Kundi and (b) Knobby Quarries in the Mary Kathleen fold belt. See Figure 3 for location. Australian map grid coordinates are indicated. The different intensities of alteration correlate with those depicted in Figure 3, except for the extremely albitized category at Knobby Quarry, in which 100 percent of the rocks at meter scales contain >80 percent albite and 100 percent combined albite, calcite veinlets, and calc-silicate alteration minerals. Calcic alteration zones shown are also intense and contain >50 percent actinolite and/or clinopyroxene, with additional metasomatic albite, scapolite, and rare biotite.The Kundi occurrence is typical of shear-related vein and alteration systems, whereas the Knobby occurrence formed in a dilatant zone located at an embayment in the metadolerite-calc-silicate rock contact. The metadolerites are inferred to have intruded at ca. 1740 Ma, whereas the veining and alteration formed primarily between 1555 and 1525 Ma according to titanite U-Pb ages and structural relationships (see text).

Curtin VG354 mass spectrometer using a Daly photomultiplier in peak jumping mode. Lead was measured at a filament temperature of about 1,400° to 1,500°C, and U was measured in metal form with a filament temperature of about 2,000°C.

Figure 8 shows our U-Pb titanite isochron plots for selected albitites from the Eastern Succession with the full data shown in Table 4. Figure 9 presents these data in the context of previously published U-Pb zircon results from selected plutons of the Williams Suite (Page and Sun, 1998; Pollard et al., 1998), recent Re-Os molybdenite and U-Pb titanite data from the Osborne deposit, and Ar-Ar results for the two most northern currently mined Fe-Cu-Au orebodies, Eloise and Ernest Henry. The oldest titanites, from the Osborne mine, were sampled from foliated albite-quartz albitite, as well as albite alteration surrounding postfoliation pegmatites (Gauthier et al., 2001; Rubenach et al., 2001). The two ages reported by Gauthier et al. (2001) and Rubenach et al. (2001) are indistinguishable at ca. 1595 Ma and are within error of the Re-Os ages for ore molybdenite. This relatively early age for albitization is consistent with the early metamorphic

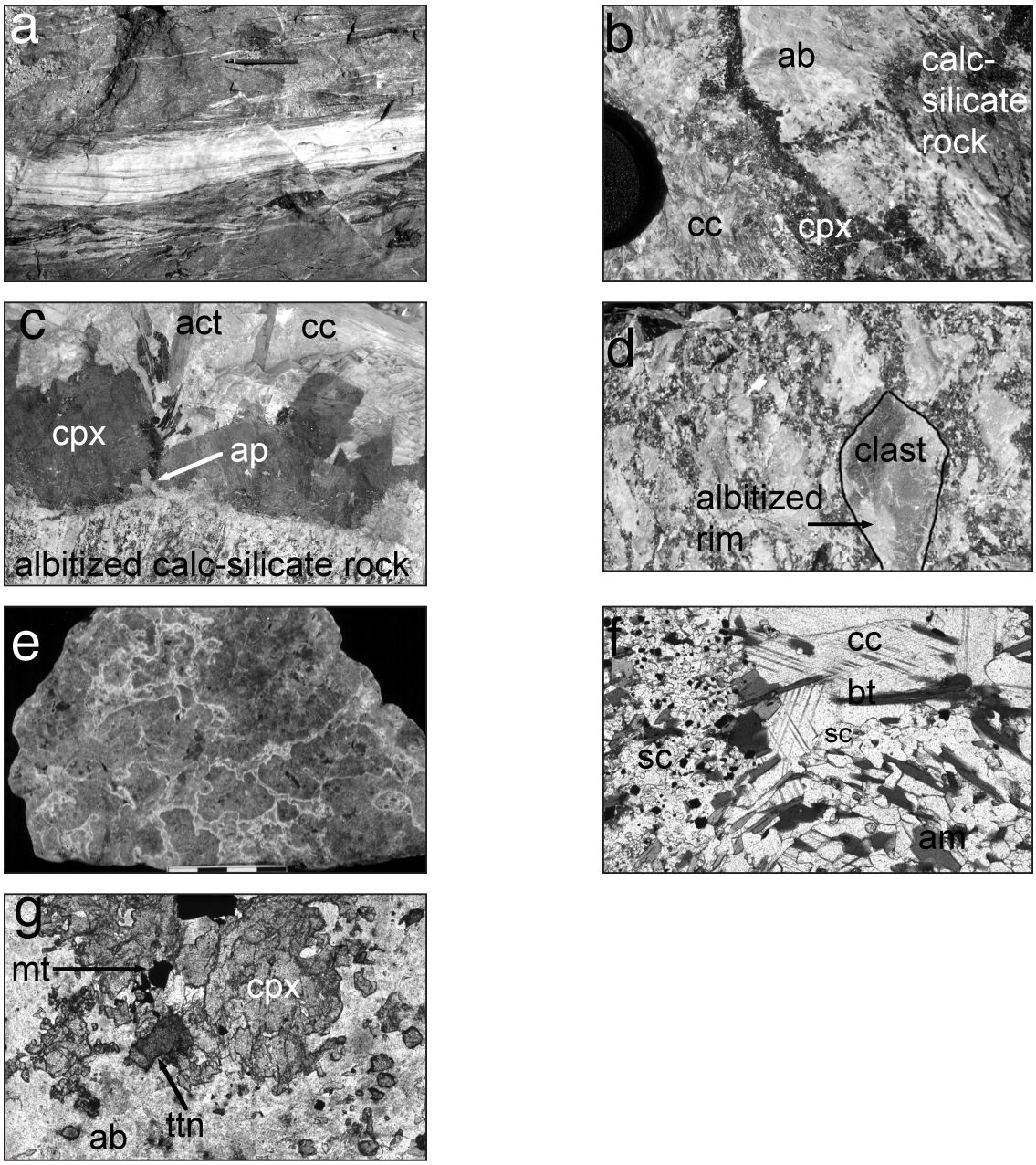

FIG. 7. Outcrop photographs and photomicrographs of albitized rocks from the Mary Kathleen fold belt and the Cloncurry district. a. Albite shear zone from the Mary Kathleen fold belt, here cutting amphibolitic metadolerite, 2 km NW of the Tribulation Quarry (location Fig. 1), pencil for scale. b. Knobby Quarry vein-related albitite (KN6) from the Mary Kathleen fold belt (location Figs. 3, 6b), showing calcite (cc) vein (left, lens cap for scale) with thin zone of clinopyroxene (cpx) and actinolitic amphibole (black) at the edge of the vein adjacent to the intensely bleached albite (ab) alteration zone (with minor clinopyroxene, calcic amphibole, and titanite). The albite alteration cuts weakly altered gray calc-silicate rock (right). c. Calcite vein in the Tribulation Quarry from the Mary Kathleen fold belt (Fig. 1), showing strongly altered bedded calc-silicate at bottom (2.5-cm coin for scale), large equant idiomorphic clinopyroxene (cpx) crystals on the vein margin, with minor elongate actinolite (act) and platy (black) biotite crystals adjacent to very coarse grained calcite (up to 1-m^3 crystals) in the vein core. d. Typical Corella Breccia from the Cloncurry district (Mt. Avarice Quarry in the Cloncurry township, Fig. 1), showing partially to completely albitized clasts in an actinolite-calcite ± quartz matrix. e. Complexly textured albite-actinolite rocks in the granite/hydrothermal transition zone in the carapace of the Mount Angelay plutonic complex, Cloncurry district (see Mark and Foster, 2000, for details). f. Photomicrograph of unaltered impure marble (sample KN 105, Table 4) from the Mary Kathleen fold belt sampled from the traverse shown in Figure 6b, showing poikiloblastic intermediate scapolite (sc) with calcite and ilmenite(?) inclusions. Calcite (cc), biotite (bt), and calcic pargasitic amphibole (am) and additional quartz and K-feldspar are also present. This rock represents a likely precursor to albitization shown in (g). g. Albitized calc-silicate (sample KN 6B, Table 4) also from the traverse shown in Figure 6b, showing total replacement of scapolite, K-feldspar, biotite, and most of the calcite by albite, clinopyroxene, titanite, and magnetite. The titanite produced by such albitization yielded an age of 1527 Ma from this sample (see Fig. 8).

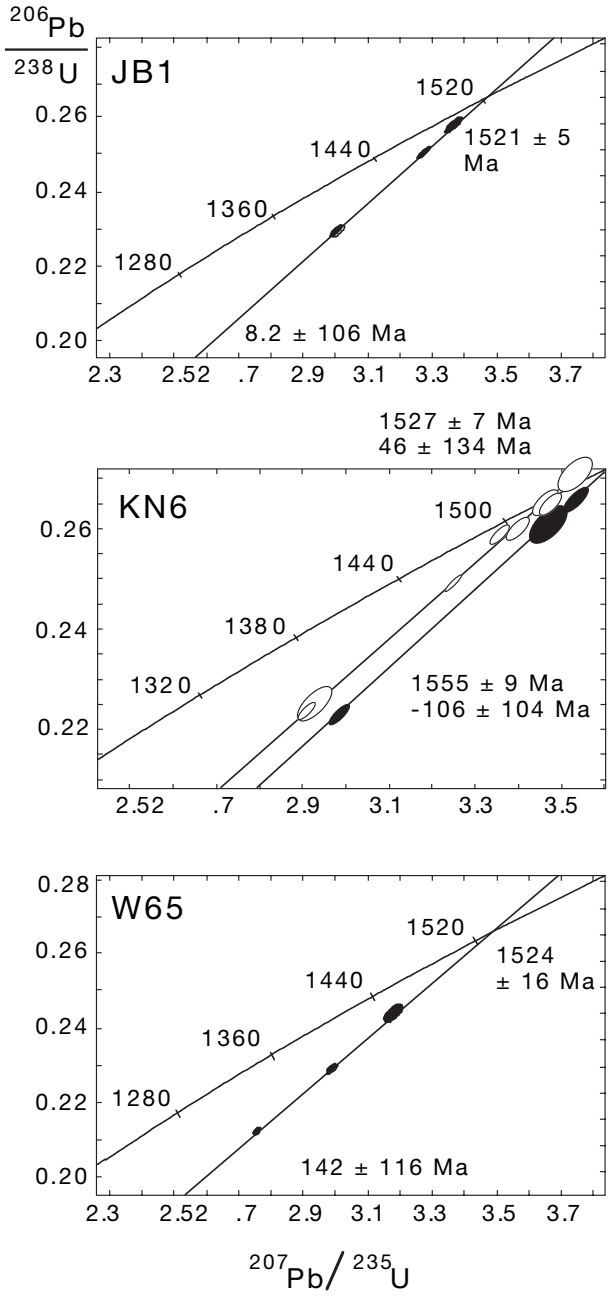

FIG. 8. U-Pb isochrons for titanites from the Eastern Succession (for sample locations see Figs. 1 and 3; for analytical methods see text). Selected titanites were all optically unzoned, free of inclusions, and not metamict. Data is shown in Table 4. Knobby albitite (sample KN6, see also Fig. 7b, g) yielded two ages as indicated, which we correlate with less abundant deformed varieties (e.g., breccias with stretched clasts) and more abundant crosscutting varieties not distinguished at the scale of Figure 6b. Sample JB1 was taken from a northerly trending intensely albitized breccia sheet at the contact between metadolerite and calc-silicate rocks, and the sample consisted of several breccia clasts all containing abundant albite and up to 5 percent titanite; the little altered rocks surrounding the breccia contain abundant biotite. Sample W65 was taken from a very similar albitized breccia cutting calc-silicate and biotite-bearing pelitic rocks. The discordant grains indicated have lower intercepts with young ages and very large errors, which we interpret to be a consequence of low-temperature, relatively young Pb or U mobility (probably surface leakage), but these have not grossly upset the systematics because both discordant and concordant grains define reliable ages from the upper intercepts, with the stated errors.

timing reported by Rubenach and Lewthwaite (2002) for albitized pelites in the Snake Creek area south of Cloncurry. Pegmatites are abundant at Osborne and are similar in emplacement age to the albitites (Rubenach et al., 2001) but are not temporally related to the younger Williams Suite. The 1555 ± 9 Ma U-Pb titanite age from the Knobby Quarry sample (KN6A) in the Mary Kathleen fold belt from this study is inferred to represent the onset of alteration associated with the 1550 to 1500 Ma hydrothermal event in this belt, which is also constrained by the 1550 ± 15 Ma age for uraninite ore from the Mary Kathleen U-REE orebody, which cuts the Mary Kathleen syncline (Page, 1983). The younger titanite ages in the Mary Kathleen fold belt, 1527 ± 7 (Knobby) and 1521 ± 5 Ma (sample JB1, near Knobby, Fig. 6b), are similar to the 1524 ± 16 Ma titanite age farther east in the Cloncurry district, as well as a major intrusive phase of the Williams Suite and several of the Ar-Ar deposit ages (Fig. 9).

Albitite Geochemistry

Table 5 and Figure 10 show results of geochemical analyses of calc-silicate rocks, psammopelitic rocks, and various intrusive rocks from the Eastern Succession, and their albitized equivalents. These data are based on systematic sampling and whole-rock XRF and INAA (neutron activation) analyses of 24 least altered rocks and 21 albitized rocks. Our sampling strategy was intended to cover the broadest possible range of starting compositions to see how different rocks responded to the albitization. Other analyses reported in Baker (1996) and Mark (1998b) show similar trends. In addition, we present results for metadiorite and a mineralization-related biotite-magnetite–altered equivalent from the Ernest Henry Cu-Au deposit (Fig. 10g). The isocon method of Grant (1986) was employed for the paired samples, or pairs of averaged samples, whereby the concentration of a particular oxide or element is multiplied by a factor for both the unaltered and altered rock in order to construct a line of best fit for the immobile elements (the isocon) on a dimensionless plot of unaltered versus altered rock. Once this line is established, a mass change can be determined, as well as the relative gains and losses of elements accompanying alteration. Errors and averaging methods are discussed for specific examples. Representative geochemical analyses are given in Table 5, and the remaining geochemical analyses used for the isocon plots are available from the authors on request.

Metasedimentary rocks

The most widespread rocks in the exposed part of the Eastern Succession are the impure marbles, calc-silicate rocks, and metasiltstones of the Corella Formation and equivalents in the Mary Kathleen Group. Away from the alteration zones, these rocks contain scapolite, biotite, calcite, quartz, microcline, calcic amphibole, clinopyroxene, and various accessory minerals, particularly titanite, apatite, allanite, and tourmaline (Table 3, Oliver et al., 1992). These starting rocks may be regarded as unaltered precursors because the high degree of preservation of volatile-sensitive metamorphic minerals and assemblages requires that the rocks did not experience significant mass changes prior to albitization.

Rocks from around the Knobby Quarry in the Mary Kathleen fold belt were sampled in a 20-m transect, with one 15-cm-wide

TABLE 4. U and Pb Abundances and Isotope Ratios from Selected Titanites in the Eastern Fold Belt

Sample no.	U (ppm)	Pb (ppm)	$^{206}Pb/^{204}Pb$	Error (%)	$^{207}Pb/^{206}Pb$	Error (%)	$^{207}Pb/^{235}U$	Error (%)	$^{206}Pb/^{238}U$	Error (%)	Corrected	$^{207}/^{206}$age	Error
W65-1	526	132	1149	1.3	0.09373	0.3	2.7594	0.5	0.2135	0.3	0.77	1503	6
w65-2	313	80	1443	3.2	0.09427	0.4	2.9902	0.6	0.2300	0.3	0.71	1514	8
w65-3	242	79	402	0.5	0.09423	0.7	3.1816	0.9	0.2449	0.5	0.71	1513	13
Kn6-1	176	58	1873	1.9	0.09475	0.9	3.5340	1.2	0.2705	0.8	0.68	1523	17
Kn6-2	242	74	3328	5	0.09648	0.5	3.5316	0.9	0.2655	0.7	0.85	1557	9
Kn6-3	191	60	3005	2.2	0.09506	0.6	3.4027	0.9	0.2596	0.7	0.77	1529	11
Kn6-4	131	47	296	0.7	0.09648	1.0	3.4681	1.3	0.2607	0.7	0.70	1557	18
Kn6-5	95	31	761	2.5	0.09505	0.7	3.4681	1.0	0.2646	0.6	0.72	1529	13
Kn6-6	188	52	1364	2.8	0.09706	0.4	2.9837	0.8	0.2230	0.7	0.88	1568	7
Kn6-7	112	33	396	1.6	0.09449	0.9	2.9280	1.5	0.2247	1.0	0.76	1518	18
Kn6-8	197	61	3003	6.7	0.09429	0.4	3.3590	0.8	0.2584	0.7	0.88	1514	7
Kn6-9	197	60	1805	1.4	0.09469	0.2	3.2470	0.6	0.2487	0.6	0.94	1522	4
Kn6-10	176	49	1275	2.3	0.09459	0.4	2.9109	0.7	0.2232	0.6	0.82	1520	8
Kn6-11	128	40	2454	7.1	0.09514	0.5	3.4696	0.8	0.2645	0.6	0.79	1531	10
Jb1-1	149.6	49	1592	1.9	0.09471	0.5	3.3755	0.8	0.2585	0.7	0.80	1522	7
Jb1-2	225.1	69	3095	2.1	0.09453	0.2	3.2740	0.5	0.2512	0.4	0.92	1519	3
Jb1-3	127.1	46	2913	1.6	0.09449	0.4	3.0290	0.7	0.2325	0.6	0.85	1518	6

Notes: Isotope data shown were corrected for blanks and common lead; analyses performed by Alexander Nemchin, Curtin University; for locations see Figure 1; analytical procedures are described in the text and sample details are in Figure 8

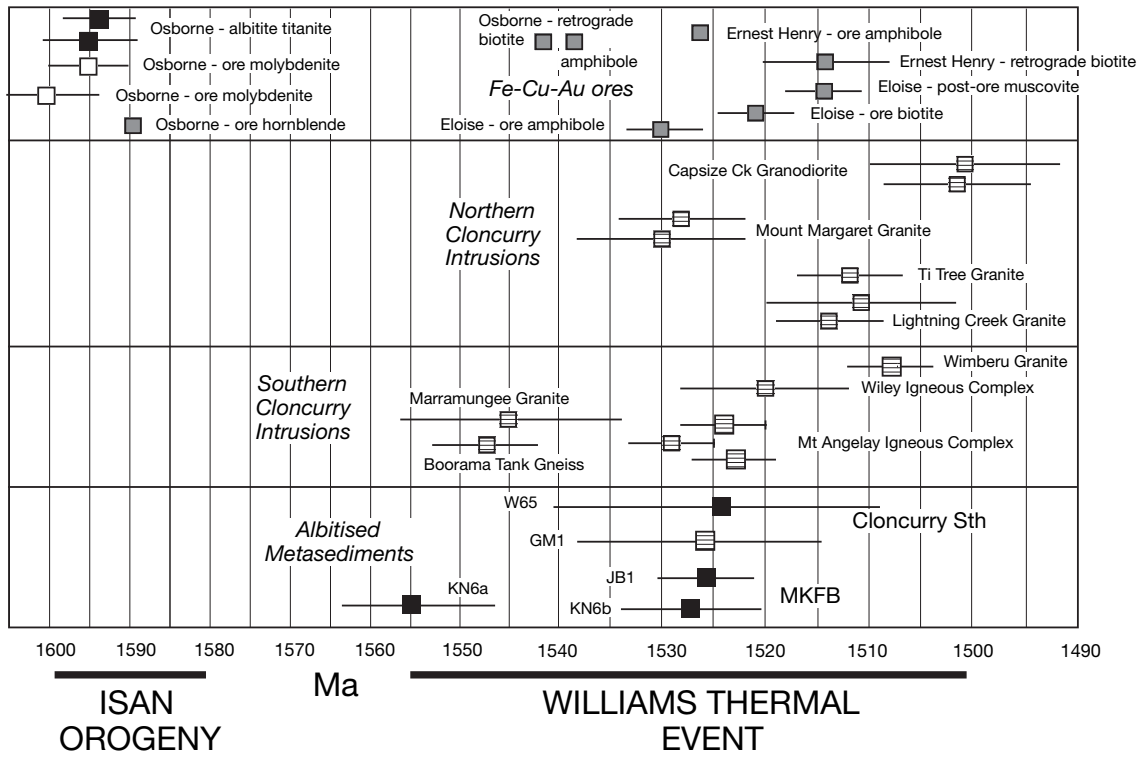

FIG. 9. Summary of geochronologic data from the Eastern fold belt, with data sources as indicated. Note that the bulk of the Ar-Ar ages for Cu-Au mineralization postdate the U-Pb titanite ages for albitization and some of the U-Pb zircon ages for granite emplacement, but given the blocking temperature differences for zircons, titanites, amphiboles, and micas, these dates are consistent with a protracted phase of intrusive activity accompanying initial albitization and then overlapping Cu-Au mineralization (e.g., Page and Sun, 1998).

TABLE 5. Whole Rock Analyses of Pairs of Less Altered Rocks and Equivalent Albitites from the Eastern Succession, along with Select Alteration Indices

Sample no.	94b	94d	S404	S253.3	219	147i	KN105	KN6B	EHD1	EHD4	42767	42741	EL079	EL116	*J1L*	*J1M*
Rock type		Alb-pelite		Alb-pelite		Alb-calc-sil		Alb-calc-sil		Alb-diorite	Qtz monz.	Alb-qtz monz.		Alb-amphib		*Bt-alb-diorite*
Location	Pelite Marra	Marra	Pelite SnkCk	SnkCk	Calc-sil MA	MA	Calc-sil Knobby	Knobby	Diorite EHM	EHM	MA	MA	Amphib Eloise	Eloise	*Diorite EHM*	*EHM*
SiO_2	75.57	73.51	56.10	65.30	63.21	59.53	46.91	55.90	62.18	58.80	66.50	68.41	55.71	60.79	*57.50*	*51.30*
TiO_2	0.51	0.40	0.64	0.70	0.57	0.62	0.39	0.46	0.90	0.85	0.57	0.63	1.08	1.04	*1.12*	*1.28*
Al_2O_3	11.91	11.36	21.70	19.50	15.37	14.25	11.50	14.24	15.78	18.37	14.96	15.69	15.9	15.72	*18.0*	*17.4*
$Fe_2O_{3(total)}$	4.36	2.40	8.29	0.47	5.85	5.66	6.11	2.74	6.18	6.25	3.81	1.99	11.85	4.5	*8.69*	*11.93*
MnO	0.05	0.02	0.05	0.01	0.06	0.07	0.23	0.12	0.03	0.07	0.02	0.03	0.19	0.21	*0.03*	*0.06*
MgO	1.01	2.47	2.22	0.28	2.90	3.87	2.05	4.48	1.83	1.79	0.95	0.77	3.67	1.46	*2.28*	*5.26*
CaO	0.42	2.24	0.35	0.65	5.58	6.55	15.50	10.13	4.08	2.65	2.02	2.47	3.97	5.47	*1.19*	*0.78*
Na_2O	1.40	6.55	0.53	10.69	1.21	4.38	5.00	7.07	5.24	8.93	4.83	8.94	3.63	7.37	*8.72*	*5.30*
K_2O	3.20	0.11	6.52	0.38	5.11	2.84	1.18	0.51	2.64	0.59	4.79	0.17	2.77	0.31	*1.01*	*4.38*
P_2O_5	0.11	0.20	0.21	0.19	0.14	0.22	0.12	0.20	0.19	0.25	0.17	0.17	0.13	0.14	*0.00*	*0.00*
Cl	na	na	na	na	0.02	0.01	0.08	0.15	0.29	0.05	0.06	0.05	na	na	*0.03*	*0.06*
LOI	2.10	0.63	2.72	0.28	2.51	0.16	10.18	4.01	0.96	1.12	0.88	b.d.	0.90	3.45	*1.23*	*2.03*
Total	100.64	99.89	99.50	98.50	102.53	98.17	99.37	100.07	100.30	99.72	99.60	99.27	99.86	100.45	*99.80*	*99.80*
Ba	na	na	875	44	na	na	320	63	489	139	1375	233	632	43	*193*	*909*
Rb	156	4	327	13	192	116	58	38	54	21	323	4	127	14	*49*	*266*
Sr	36	20	33	52	80	80	79	60	136	130	139	132	99	51	*104*	*224*
Pb	na	na	6	6	3	2	na	na	4	4	17	17	bd	bd	*3*	*bd*
Zr	211	212	131	162	200	209	106	97	174	207	343	550	139	186	*163*	*192*
Nb	na	na	21	18	na	na	na	na	16	12	31	39	10	13	*13*	*14*
Y	26	24	24	16	29	22	20	60	34	26	31	57	30	28	*26*	*17*
La	na	na	na	na	na	na	na	na	41	53	104	99	na	na	*31*	*29.6*
Ce	na	na	na	na	na	na	92	103	88	82	261	195	na	na	*65.8*	*62.6*
Sc	na	na	20	9	na	na	17	21	13	18	6	5	22	22	*4*	*4*
V	na	na	106	32	na	na	62	20	66	62	47	27	268	162	*157*	*225*
Cr	na	na	101	92	65	57	26	64	8	12	156	12	46	41	*bd*	*19*
Co	na	na	17	21	28	9	20	31	13	10	7	27	42	18	*7.31*	*16.7*
Ni	na	na	34	4	24	24	23	7	5	11	8	6	38	14	*24*	*48*
Cu	na	na	7	8	10	15	5	5	20	23	13	10	79	76	*10*	*5*
Zn	na	na	49	5	7	0	5	7	58	26	20	24	33	19	*15*	*25*
Ga	na	na	34	21	19	18	16	15	21	27	9	13	21	22	*26*	*31*
100Na/(Na + K)	30.4	98.3	7.5	96.6	19.1	60.7	80.9	93.3	66.5	93.8	50.2	98.1	56.7	96.0	*89.6*	*54.8*
100(Na + Ca)/(Na + Ca + K)	36.3	98.8	11.9	96.8	57.0	79.4	94.6	97.1	77.9	95.2	58.9	98.5	73.3	97.6	*90.8*	*58.1*
100Na/(Na + Fe)	24.3	73.2	6.0	95.8	17.1	43.6	45.0	72.1	45.9	58.8	55.9	81.8	23.4	62.1	*50.1*	*30.8*

Notes: Major element oxides in wt percent, minor elements in ppm; other analyses available from the authors upon request; abbreviations: alb = albitized, amphib = mafic meta-igneous amphibolite, calc-sil = calc-silicate rock, monz. = monzonite, Marra = Marramungee Creek, SnkCk = Snake Creek, EHM = Ernest Henry mine, MA = Mt. Angelay, locations in Figure 1; LOI = loss on ignition, b.d. = below detection limit, na = not analysed; the two samples in italics represent the transition from amphibolite (already partly albitized) to the biotite-magnetite altered equivalent in the proximal alteration halo of the Ernest Henry orebody (Fig. 5), for which most trends are opposite to those determined for albitization (see text)

calc-silicate dominant layer tracked from unaltered, well-bedded rock into its albitized equivalent (Fig. 6b). At the transition to the most intensely albitized rocks, it was no longer possible to discern this particular layer, and results for this part of the transect are averaged (Fig. 10a). Confidence that the transition was appropriately sampled is based on the distinctive Ti/Zr and Ti/Al ratios in the altered and least altered equivalent. Figure 10b shows results for a pair of closely spaced samples (KN6A and KN6B, Fig. 7b). Al, Zr, Ti, Ga, Si, and Co all show immobile behavior in the altered examples (Fig. 10a, b). The best fit isocon for the averaged dataset (Fig. 10a) suggests that albitization occurred at near-constant mass or with a slight mass increase ($F_m > 1$, where F_m = mass final rock/mass initial rock), whereas there was a slight mass decrease in the transition from samples KN6A to KN6B in Figure 10b. It is clear that the altered rocks have gained Na and lost Fe, Mg, K, Mn, Ni, V, Zn, Nd, S, Rb, and Ba. The patterns for total mass change and for Cu and Ca are inconsistent between Figure 10a and b. These two elements are apparently recording differential mobility across a range of scales (from meters in Fig. 10a to centimeters in b). The variations are not surprising given the abundance of calcite veinlets accompanying albitization, which locally contain minor chalcopyrite (see below).

A second set of albitized calc-silicate rocks was sampled in the Mount Angelay area where the rocks could be readily separated into unaltered and altered types but could not be readily tracked from one to the other due to synalbitization brecciation. For these five samples, we averaged the three unaltered rocks and compared them with the average of the two albitized equivalents in Figure 10c, with the variability in precursor compositions represented by the standard deviation between the samples (error bars). The isocon plot shows that Al, Si, Ti, and Ga were immobile, generally consistent with the observations from the Mary Kathleen fold belt. Na, Ca ± Cu, and Mg were gained during albitization, and K, Zn, Y, Rb, and Pb were lost. Other trace elements not shown in this plot had very large standard deviations. One of the least altered samples (sample 219, with an assemblage of scapolite, biotite, quartz, K-feldspar, clinopyroxene, titanite and minor epidote, magnetite and actinolite), characteristic of the majority of least altered calc-silicate rocks in the Cloncurry district, was used as a calc-silicate reference material for the geochemical modeling presented below.

Albitized pelites from the Snake Creek anticline (Rubenach and Lewthwaite, 2002) are present in shear zones, in alteration veins surrounding the shear zones and related quartz veins, and in more broadly distributed zones along the contacts with mafic amphibolites. Average albitized pelites sampled at five locations spaced over several kilometers (Rubenach and Lewthwaite, 2002), compared with their least altered equivalents (Fig. 10d), show constant Al, Si, Ti, Ga, Zr, Y, Cr, and Nb and a mass increase of approximately 4 percent. Na and Ca are enriched, and K, Fe, Rb and Mn are clearly depleted. The Ca enrichment is similar to that observed by Williams (1994) and, as there is no local source for the Ca, must reflect transport of this component from outside the sequence via the infiltrating fluid.

Igneous rocks

Pristine and albitized diorites were sampled near Ernest Henry (Fig. 5), and the nine samples were separated into three least altered, three moderately altered, and three intensely altered. Ga, Si, Al, Ce, and La remain immobile even in the intensely altered rocks. Ti, Cu, and Zn have large standard deviations, although Ti was most likely immobile based on the other samples. Na was added, particularly in the intensely altered rocks. Fe, Mg, V, and Y were nearly immobile in the moderately altered rocks but were significantly depleted in the intensely altered rocks, and there is a suggestion also that Al may have been slightly depleted in the most altered rocks. K, Ba, Ca, Sr, and Rb were all lost from the moderately altered rocks and are extremely depleted in the most altered rocks. Similar trends (but with large standard deviations for several trace elements) are shown by the albitized quartz monzonite and syenogranite samples from Mount Angelay (Fig. 1, Table 5). The most mafic rocks analyzed were a pair of samples from the Eloise Cu-Au deposit (Baker, 1996), a little altered amphibolite and a strongly albitized equivalent (Fig. 10f). A very well constrained isocon is defined on the basis of immobile Al, Ti, Y, Cu, Ga, and Sc, with near-immobile Si, Cr, and Mn and little total mass change between the precursor and albitized equivalent (ca. 3% mass increase). K, Rb, and Ba are extremely depleted, Fe, Ni, V, Sr, Mg, and Co are moderately depleted, and Na, Ca and Zr are enriched. We interpret the apparent Zr enrichment as a spike effect due to irregular distribution of Zr in accessory minerals spaced farther apart than the sampling distance.

Ore-related alteration

Magnetite-biotite alteration is a common feature of the proximal alteration halo of the Cu-Au orebodies (Table 2). In order to compare the albitization with the ore-forming process, we compared one example of the Ernest Henry Diorite to its magnetite-biotite–altered equivalent (Figs. 5, 10g). Because our sample pair involves an intrusive igneous rock with a well-studied paragenetic history (Mark et al., 2000) we are confident that the changes measured do not relate to primary iron enrichments. Comparison of Figure 10e and g shows that the effects of ore-related potassic alteration are dramatically different from albitization of the same rock, with trends for individual elements mostly being the opposite between the two alteration types. Ca is the only obvious anomalous element, being lost from both albitized and biotite-magnetite–altered diorite. Calcite is found in abundance, however, as vein infill to crackle-brecciated diorite on the edge of the ore deposit some tens of meters from these samples.

Summary

Mass changes for the major elements associated with albitization are summarized in Figure 11. Aluminum, Ga, Ti, and Zr are consistently immobile, and Si is also mostly immobile. The very local presence of titanite in some veins suggests local mobility of Ti. Consistent gains in Na are matched by depletions in K, alkali earth elements, Zn, and Fe, the latter being very mobile (depleted) in intensely altered rocks. Uranium and Pb are generally low in abundance but are depleted in the most altered rocks, as are Cr, Mn, V, and Ni. Variable gains and losses are indicated for Ca, Cu, and Mg. The sample suites with 3 to 12 percent mass gains all show increases in Ca and Mg, and samples with 2 to 10 percent mass loss

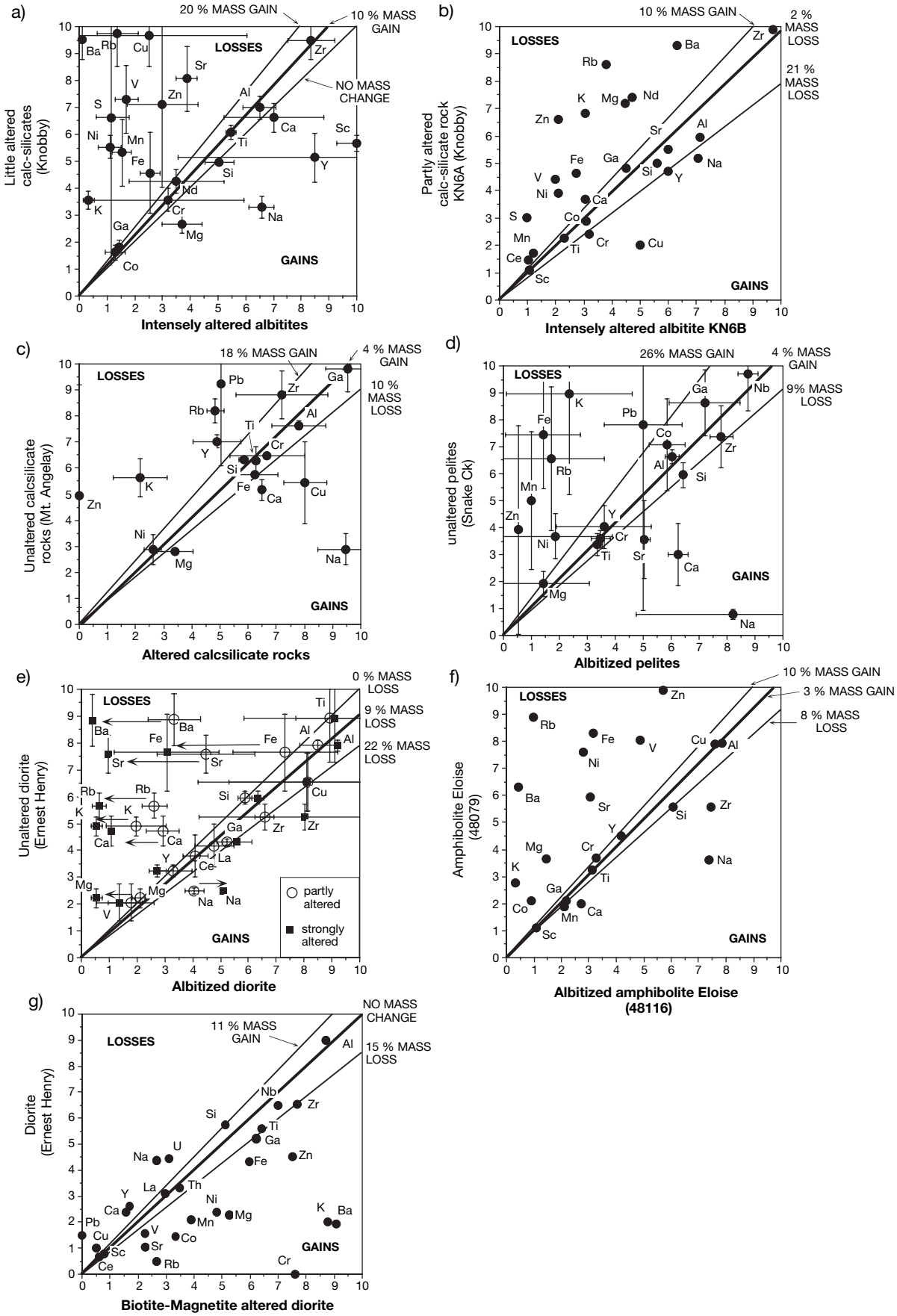
a)
20 % MASS GAIN
10 % MASS GAIN
NO MASS CHANGE
LOSSES
GAINS
Little altered calc-silicates (Knobby)
Intensely altered albitites
b)
10 % MASS GAIN
2 % MASS LOSS
21 % MASS LOSS
LOSSES
GAINS
Partly altered calc-silicate rock KN6A (Knobby)
Intensely altered albitite KN6B
c)
18 % MASS GAIN
4 % MASS GAIN
10 % MASS LOSS
LOSSES
GAINS
Unaltered calcsilicate rocks (Mt. Angelay)
Altered calcsilicate rocks
d)
26% MASS GAIN
4 % MASS GAIN
9% MASS LOSS
LOSSES
GAINS
unaltered pelites (Snake Ck)
Albitized pelites
e)
0 % MASS LOSS
9 % MASS LOSS
22 % MASS LOSS
LOSSES
GAINS
partly altered
strongly altered
Unaltered diorite (Ernest Henry)
Albitized diorite
f)
10 % MASS GAIN
3 % MASS GAIN
8 % MASS LOSS
LOSSES
GAINS
Amphibolite Eloise (48079)
Albitized amphibolite Eloise (48116)
g)
NO MASS CHANGE
11 % MASS GAIN
15 % MASS LOSS
LOSSES
GAINS
Diorite (Ernest Henry)
Biotite-Magnetite altered diorite

(and inferred volume decrease) are correspondingly depleted in Ca and Mg. This suggests that Ca- and Mg-bearing minerals in microveinlets and microbreccia matrix are at least partly responsible for the variation in F_m. Cu may have been mobile during albitization, but the variability may reflect the role of several Cu-bearing minerals, and the albitization is not considered to have been responsible for significant mass transfer of Cu. Finally, excepting Cu and Ca, elements gained during albitization were apparently lost during ore-related potassic alteration and vice versa (Fig. 10e, g).

Evidence from Carbon and Oxygen Isotopes in Calcite

The close association between albitization and calcite and/or actinolite veining across the district in the Corella Formation and equivalents (Oliver et al., 1990, 1993; Marshall and Oliver, 2002) means that the carbon and oxygen isotope systems can be used to assess fluid-rock interaction during albitization, particularly because calcite is also a common constituent of the primary, least altered metamorphosed calc-silicate rocks and marbles of the sequence. All carbon and oxygen results are from calcite mineral separates from rocks or veins (and breccia infill), analyzed using the method of McCrae (1950) in the Monash University stable isotope facility. The $\delta^{18}O$ and $\delta^{13}C$ values are reported relative to standard mean ocean water (SMOW) and Peedee belemnite (PDB), respectively. We present raw calcite data here because all of the samples are from high-temperature metamorphic rocks or veins, with calcite formation temperatures (or recrystallization temperatures in the least altered metamorphic rocks) in the range of 450° to 600°C (from isotope pairs and mineral geothermometry). Across this temperature range, and with calcite present as the only carbonate, fractionation between calcite and H_2O-CO_2 fluids has only a small temperature dependence (for fluids with 10 mol % CO_2, $\Delta^{13}C_{calcite\text{-}CO_2}$ = –2.6‰ at 450°C and –1.3‰ at 600°C; $\Delta^{18}O_{calcite\text{-}H_2O}$ = 2.0‰ at 450°C and 0.3‰ at 600°C; Friedman and O'Neil, 1977; Sharp and Kirschner, 1994). The lack of CH_4 in the associated fluid inclusions, coupled with the high temperatures, means that large effects should not be observed as a function of C isotope partitioning between these species. Most of the variations depicted in this dataset are much larger than possible variations due to temperature gradients, as discussed below.

New and previously published carbon and oxygen isotope data from least altered, albitized, and mineralized rocks in the eastern Mount Isa block are presented in Figure 12. The $\delta^{18}O$ and $\delta^{13}C$ values for calcite from least altered marbles and calc-silicate rocks cluster around 20 and –2 to +2 per mil, respectively (Fig. 12a), and are consistent with expected values for pristine, metamorphosed Proterozoic marine carbonates (Valley, 1986; Oliver et al., 1992). The difference betweeen starting compositions for Cloncurry and Mary Kathleen carbonate rocks are either due to primary differences in the sedimentation environment or, more likely, reflect the more extensive metamorphic decarbonation of the Mary Kathleen rocks, prior to the alteration (Marshall, 2003). Samples gathered from zones of weak to moderate albitization (e.g., Figs. 3, 6) typically show textural evidence for two calcite generations, a relict peak metamorphic variety and a second variety comprising veinlets, overgrowths, and ragged patches cutting the older carbonate (Oliver et al., 1993; Marshall, 2003). In the Cloncurry district marbles, albitization involves destruction of biotite in the marble, and biotite-absent marbles have lower $\delta^{18}O$ values than unaltered marbles and calc-silicate rocks. In both cases (gray symbols, Fig. 12a), the data are interpreted to reflect mixtures of different proportions of earlier and later calcite with substantially different $\delta^{18}O$ values. Weakly to moderately altered calc-silicate rocks from Cloncurry are similarly depleted in ^{18}O relative to precursors and also show ^{13}C depletions of up to 4 per mil. Both strongly altered calc-silicates from the Mary Kathleen fold belt and albite breccias from Cloncurry retain little or no metamorphic calcite. Samples were analyzed from intensely bleached rocks adjacent to large vein or breccia systems, and the original differences between the Mary Kathleen fold belt and the

FIG. 10. Isocon plots (after Grant, 1986) constructed for individual pairs or averaged sets of rocks, comparing little altered precursors with albitized equivalents (a–f) and weakly altered diorite with its magnetite-biotite–altered equivalent in the Ernest Henry deposit (g). Sample locations are shown in Figures 1, 5, and 6b except where otherwise noted. The raw data is presented in Table 5. Mulitplication factors are used for each element rather than log scales or the raw data, as this allows for easier discrimination of mobile and immobile elements and the ability to plot standard deviations as error bars. In each case the main isocon (heaviest line) was determined by a visual best fit to constant Al and Ti ± Ga, Zr, and Si. The lighter lines show a range of possible isocons for which other elements could also have been immobile. Their positions were determined by a visual best fit to include elements most likely to also be immobile in addition to Al and Ti, particularly Ga, Zr, Si, Y, La, Ce, Nb, and Nd, unless these latter elements already lay close to the main isocon. Because these are ratio plots in which we have arbitrarily nominated multiplication factors in order to distribute the elements as broadly as possible across the diagram, statistically determined best fits are invalid. Alternate isocons could be constructed for immobility of one particular element, such as Al or Ti. a. Averaged data comparing three little altered calc-silicate rocks with three albitized equivalents, Knobby Quarry. F_m = 1.1 ± 0.1, where F_m (the mass factor) is the ratio of the total mass of the altered rock to that of the less altered equivalent, determined solely from the slope of the isocon, giving some idea of whether dilation ($F_m > 1$) or dissolution ($F_m < 1$) accompanied the alteration. b. Comparison of samples KN6A and KN6B, where KN6B is a 2-cm-wide intensely altered rim (adjacent to a calcite vein) overprinting partly altered KN6A calc-silicate rock. F_m = 0.98 ± 0.16. c. Averaged data comparing three little altered calc-silicate rocks with two albitized equivalents from the Mount Angelay area, Cloncurry district (data from Mark, 1998b). F_m = 1.04 ± 0.12. d. Averaged data comparing five little altered pelites from the Snake Creek area with three altered equivalents (outcrop descriptions in Rubenach and Barker, 1998, and Rubenach and Lewthwaite, 2002). F_m = 1.04 ± 0.17. e. Averaged data comparing three diorites with four moderately altered equivalents and three intensely altered equivalents, from near the Ernest Henry mine, along the traverse indicated in Figure 5. F_m = 0.91 ± 0.10. f. Comparison of a mafic amphibolite with its albitized equivalent, Eloise mine (data from Baker, 1996). F_m = 1.03 ± 0.06. g. Comparison of a weakly albitized diorite with a magnetite-biotite–altered equivalent from the Ernest Henry mine, showing the opposite trends to those indicated for the albitization (see text). F_m = 1.00 ± 0.13.

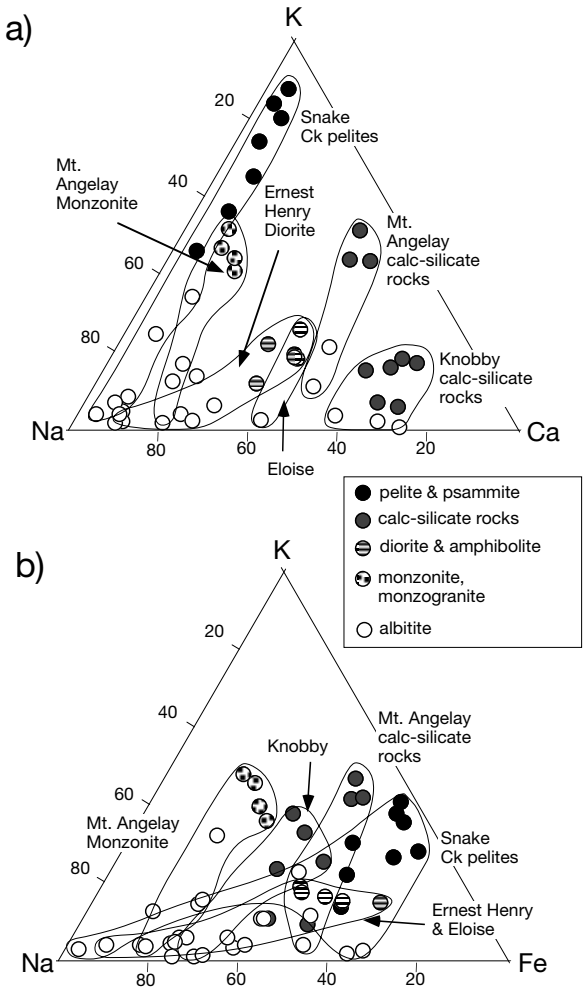

FIG. 11. Summary triangular diagrams for albitization, calculated using raw oxide data (i.e., assumes total mass changes are negligible; see Fig. 10) from Table 5 and other unpublished data. a. CaO-Na_2O-K_2O. b. Na_2O-K_2O-Fe_2O_3 (all Fe determined as Fe_2O_3). Outlined fields enclose least altered rocks (darker dots) and their albitized equivalents (white dots) from various locations, as indicated. Some rocks show little relative decrease in Ca or Fe, but others show depletions in all of K, Ca, and Fe, and all rocks show an increase in Na/K ratio with albitization.

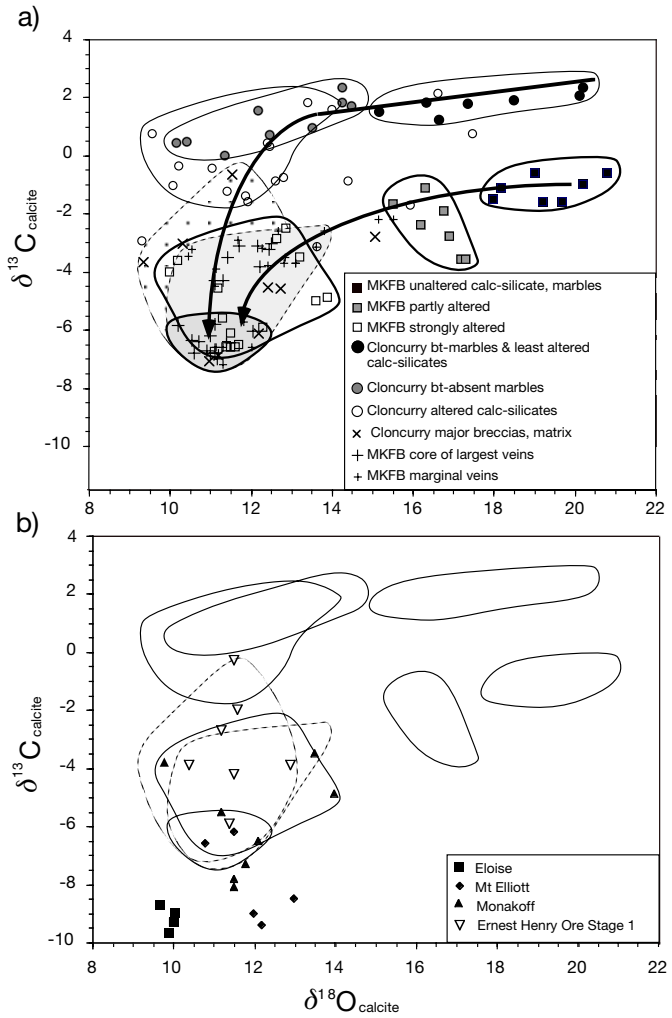

FIG. 12. Calcite mineral separate stable isotope data ($\delta^{13}C$ relative to PDB and $\delta^{18}O$ relative to SMOW) from unaltered, albitized, and mineralized rocks of the Eastern Succession. Sample locations are indicated in Oliver et al. (1993) and Marshall (2003) and are shown generally in Figure 1. a. Least altered calc-silicate rocks and marbles (black symbols), with typical marine carbonate values modified slightly by prealteration regional metamorphism, shift toward lower values with partial albitization and veining (gray symbols), and converge upon magmatic values (open symbols and crosses) in major calcite veins and breccia systems. Heavy outlined areas are from the Mary Kathleen fold belt data (Oliver et al., 1993); lighter outlines are from the northern Cloncurry district (Marshall, 2003). b. Calcite mineral separate stable isotope data from the major Fe oxide-Cu-Au ore deposits discussed in the text; data are from Davidson and Garner (unpub. data, 1997), Twyerould (1997), Mark et al. (2000), and Marshall (2003). Outlined areas are the main fields from Figure 12a, for comparison.

Cloncurry district are not apparent in these samples, with isotopic compositions of calcite in both sets of strongly altered rocks clustering around $\delta^{18}O$ = 11.5 per mil and $\delta^{13}C$ = –4.5 per mil. In the Mary Kathleen fold belt, the most albitized calc-silicates and marbles are cut by networks of calcite venlets and veins up to 2 cm thick, and these latter veins are isotopically indistinguishable from calcite extracted from the rocks themselves.

The lowest values from the district are found in samples from the Knobby and Tribulation Quarries in the Mary Kathleen fold belt and the core of the largest breccia bodies in the Cloncurry district (heaviest shaded area in Fig. 12a). The Knobby and Tribulation results are notable in that the samples come from the core of very large podiform calcite veins (Figs. 6, 7c). The trend from preserved marble signatures through to veins with the lowest $\delta^{18}O$ and $\delta^{13}C$ values correlates with proximity to the core of the largest veins or breccia systems. Thus the alteration maps shown in Figures 3 to 6 are essentially maps of C and O isotope depletion, and the isotopic zonation is interpreted to closely match the position of albite alteration fronts. The overall trends cannot be explained by temperature, devolatilization, or fluid composition effects. The characteristic L-shaped depletions in Figure 12a are consistent with infiltration of fluids of low X_{CO_2} in which rock ^{18}O is depleted substantially before ^{13}C (cf. Rumble, 1982; Valley, 1986).

Previously published data from selected Cloncurry district Cu-Au deposits and new calcite results from Ernest Henry are shown in Table 2 and Figure 12b. Ernest Henry results are indistinguishable from the intensely altered albitites and associated large calcite veins elsewhere in the district. Data from Mount Elliott, Eloise, and Monakoff (the latter being the nearest Cu-Au deposit to Ernest Henry, Figs. 1, 2) are similar to the results from the most ^{18}O depleted calcite vein samples from the entire district but have slightly lower $\delta^{13}C$ values. Notably, all of the data except for these three deposits are for samples from the Corella Formation or equivalent (calc-silicate–dominated) rocks of the Mary Kathleen Group. Mount Elliott, Eloise, and Monakoff are hosted in the Soldiers Cap Group, with Monakoff and Mount Elliott being dominated by pelitic, locally carbonaceous metasedimentary rocks and Eloise by a mixture of metasedimentary rocks and mafic amphibolites. Although some of the deposits are hosted in carbonaceous rocks, fluid inclusion data indicate that CH_4 is particularly scarce, and locally hematite and calcite form daughter minerals in fluid inclusions, indicating fairly oxidized conditions (e.g., Williams et al., 2001). Therefore, although some spread in the data may be related to different fluid sources, the majority of the samples indicate relatively isotopically homogeneous metasomatic fluids.

Geochemical Modeling

Hydrothermal geochemical modeling of fluid-rock reaction is a powerful way to test hypotheses concerning the source and reaction paths of metasomatic fluids. It has the capacity to reveal aspects of progressive fluid-rock reaction, the effects of differing P and T, variations in initial starting fluid composition, and the composition of different fluids equilibrated with different rocks. The results of the modeling can also be compared with fluid inclusion studies. Principles of this style of analysis in mineralized systems have been demonstrated by Reed and Spycher (1985), Heinrich et al. (1995, 1996), Borisov and Shvarov (1998), and Cooke and McPhail (2001), among others. Here we have simulated the albitization process using the software HCh (Shvarov, 1999; Shvarov and Bastrakov, 1999). The HCh package permits equilibrium-dynamic modeling of hydrothermal systems and processes using the free-energy minimization technique (Shvarov, 1978, 1999), rather than the log K method. HCh can be used across a temperature range of 0° to 1,000°C and pressures up to 500 MPa, within the limitations of the Helgeson-Flowers-Kirkham model, and for fluid salinities limited by the extended Debye-Hückel equations. The package can be obtained from Geoscience Australia (http://www.ga.gov.au/rural/projects/1007080747_28318.jsp). The model calculations were completed using the Geoscience Australia version of the UNITHERM database, which is included with the software, and the description of the software and database is detailed in Shvarov and Bastrakov (1999; a version of this database can be obtained by contacting E. Bastrakov at Geoscience Australia, through the web site indicated above). In the UNITHERM database, mineral thermodynamic data were adopted from self-consistent datasets compiled by Berman (1988) for aluminosilicates, with corrections for K and Na minerals suggested by Sverjensky et al. (1991), and the rest of the mineral data sourced mostly from the ETH version of SUPCRT (Pokrovskii et al., 1998). Most of the aqueous species were adopted from the ETH version of SUPCRT (Pokrovskii et al., 1998), complemented by data of Shock et al. (1997) and Sverjensky et al. (1997) for Fe and Cu complexes. Mineral solid solutions were derived using an ideal mixing-on-sites model (e.g., Powell, 1977). In the output plots in this paper, except for plagioclase, we have combined the minerals of solid-solution series without specifying the specific mineral compositions.

The simplest equilibrium calculations to model albitization were completed in a single mixing mode, an approach similar to one used by Heinrich et al. (1995, 1996). Rock is dropped into fluid (Fig. 13a) in order to avoid problems associated with initial low fluid/rock ratios for which ionic strengths can be too high for the valid range of available thermodynamic data. After an aliquot of rock has been added to the fluid, the equilibrium state is calculated by adjusting the proportions and compositions of mineral phases and by concomitantly adjusting the fluid composition to minimize the Gibbs free energy. There is not a great physical significance to the zonation produced in such models; rather they are simply tests of possible alteration assemblages that might pertain to a range of fluid fluxes. However, there is some geologic basis for choosing such simple models—the distribution of alteration around veins, with the largest veins showing the largest ^{18}O and ^{13}C depletions relative to the wall rocks, suggests that the fluid was rapidly introduced to the system via these fractures and attempted to equilibrate with the wall rocks via diffusion and infiltration of components between the wall rocks and the fluid-filled cracks. The size of the fracture and the flow rate of fluid in that fracture would have dictated the degree of reaction. Simulated alteration zones are very similar to those observed in the field (see below). This simplistic modeling approach is enhanced by knowing the starting composition of the unaltered rock and by being able to compare the output to the known compositions of the altered rocks. Similarly, data from fluid inclusions may be used to populate parts of the models or for comparison with model results.

The second type of model may be termed a "reactor," in which an algorithm is constructed that approximates a proper flow-through simulation, where fresh fluid is continually added to one end of an infiltration column (Fig. 13b). Stale fluid leaving a reactor site infiltrates the next reactor where it is modified further. Influx of fresh fluid pushes the previously modified fluid ahead so that it can react with fresh rock. Two types of reaction fronts are apparent in our models: a pseudofront beyond which the infiltrating fluid has not physically passed, and fronts in the true Korzhinskii (1970) geochemical sense, which occur along the flow path as a consequence of one or more minerals reaching or exceeding their solubility limit. A horizontal section through the output matrix is then a snapshot of the system at a moment in time. This reactor-type approach (Heinrich et al., 1996) is an approximation to reactive transport modeling (e.g., Ferry and Dipple, 1991; Dipple and Ferry, 1992) in terms of the zonation of mineral assemblages, with the limitation that real dimensions and the effects of kinetics cannot be adequately included. In theory, reactor-type models converge upon true reactive transport only when the aliquot size or reaction step is infinitesimally small (cf. Blattner and Lassey, 1990). However, the infiltration of

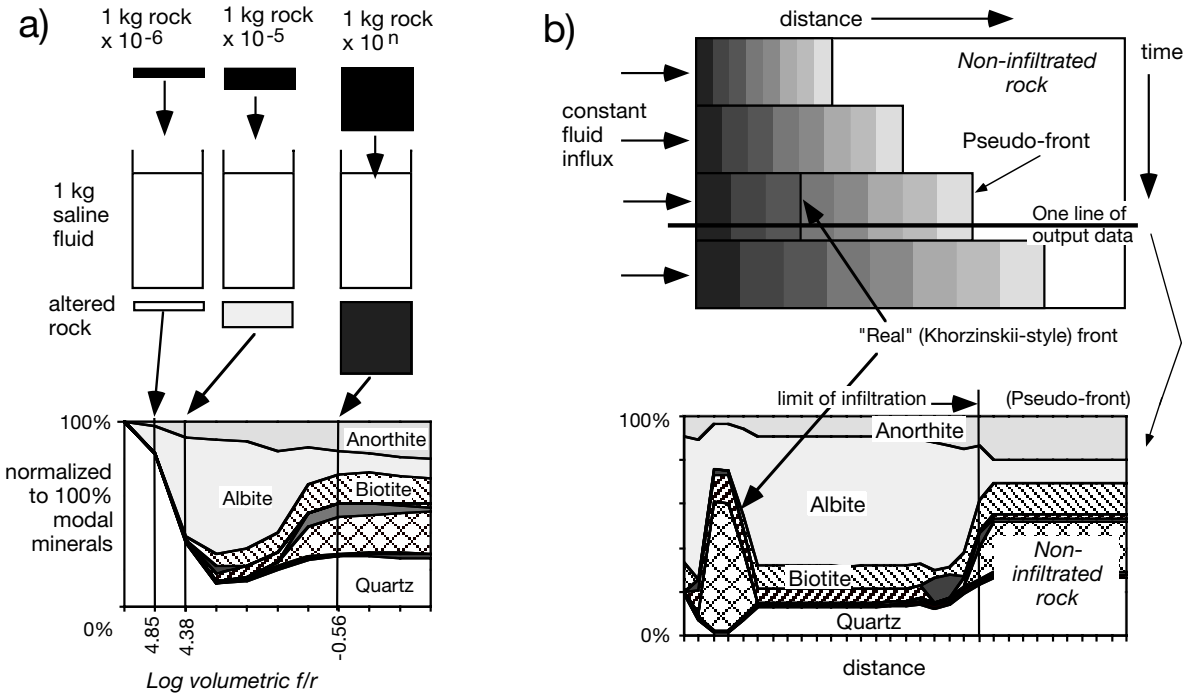

FIG. 13. Conceptual models showing the techniques used in the geochemical simulations of fluid-rock interaction, using HCh (Shvarov and Bastrakov, 1999). a. Simple aliquot-type mixing of different masses of rock with a set mass of fluid, equilibrated to produce individual outputs of altered rock assemblages, which are recalculated from moles to volumes using mineral molar volume data and plotted as a function of volumetric fluid/rock ratio (f/r). b. A flow-through model which is a closer approach to reactive transport models (cf. Heinrich et al., 1996). Khorzinskii-type fronts correspond to specific solubility limits of different minerals in the moving fluid column, whereby position is a function of the fluid flux and the specific fluid-rock partitioning for the minerals of interest. Also shown is a pseudofront, which is a realistic simulation of the boundary between infiltrated and noninfiltrated rock. Such a front is dependent on the total fluid flux, which defines the distance of the front from the inlet position but is also dependent on the assumption that beyond the front, there is no reaction and therefore no capacity for metasomatic reactions to create or destroy any permeability. Assemblages beyond the pseudofront would be considered rock buffered or least altered. This corresponds to the concept of reaction-enhanced permeability and coincident isotopic and geochemical fronts developed by Cartwright (1997). One horizontal line of output data from the computations (as depicted in Figs. 16 and 17) corresponds to a spatial array of alteration zones at a particular time that can be compared to alteration maps; output derived from vertical lines would correspond to the temporal sequence at one point in space that could be compared to a paragenesis.

fluid into rock that was not previously fluid saturated does not readily lend itself to a conventional Korzhinskii-type interpretation of reaction fronts nor to conventional reactive transport models. The algorithm we used approximates a reaction-enhanced permeability in which isotopic and geochemical pseudofronts would be coincident, as noted in detail by Cartwright (1997). Such calculations can then provide good approximations of realistic physical situations around veins in which the previous rock was essentially impermeable.

Model inputs

Model input rocks (calc-silicate Mount Angelay 219 and pelite Snake Creek S404, Table 6) were selected from those presented in Table 5. We also include an analysis of the Mount Angelay quartz monzonite (42767) in order to determine one possible input fluid composition (see below). We obtained poor model results, not presented here, from albitization of intermediate to mafic rocks (Ernest Henry diorite, Eloise amphibolite) containing abundant complex amphiboles (hornblende, hastingsite, pargasite), because inadequate activity-composition models resulted in artificial partitioning of alumina and silica into other phases. Inputs are specified as whole-rock oxides in the compositional space Si-Al-Ti-Fe-Mg-Ca-Na-K-C-H-O-S. Ti in this context acts as a completely immobile element by default as there are no soluble Ti species in the fluid database nor have we included any solid-solution models pertaining to Ti (such as Ti in biotite).

The composition of the best possible model input fluids was based on associated mineral assemblages, fluid inclusion data, and iterative modeling. One possible approach could be to take fluid inclusion data from the top of an intrusion believed to have caused albitization, such as the Mount Angelay quartz monzonite (Mark and Foster, 2000). However, the difficulties associated with using fluid inclusion data directly are (1) uncertainty about whether the analyzed fluid inclusion represents the bulk composition of the infiltrating fluid initially out of equilibrium with the rocks or the product of local rock-fluid equilibration; (2) the common occurrence of CO_2-rich inclusions, locally in the same trails as primary hypersaline fluids, raising the possibility that the hypersaline fluid

TABLE 6. Compositions of Rocks Used in HCh Models

	MA monzonite [1]	MA calc-silicate rock [4]	Snake Ck Pelite [5]
H_2O (g)	8.8	12	22
SiO_2 (g)	665	632.1	591
TiO_2 (g)	5.7	5.7	6.4
Fe_2O_3 (g)	20.6	22.3	-
FeO (g)	17.5	36.2	74
MgO (g)	9.5	29	22.2
Al_2O_3 (g)	149.6	153.7	217
CaO (g)	20.2	55.8	3.5
Na_2O (g)	48.3	12.1	5.3 §
K_2O (g)	47.9	51.1	65.2
C (mol)	-	-	0.4
CO_2 (mol)	-	0.32	-
Log $Na/K_{m(aq,\ total)}$	0.48	–0.02	–1.90 §
pH	5.12	6.13	4.06
$\log f_{O_2}$	–19.9	–20.1	–24.4

Notes: Compositions were derived from data shown in Table 4 and are expressed as g/kg for the solid components and mineral-bound volatiles; Na/K, pH, f_{O_2} were derived by equilibrating an excess of each rock with a 3*m* HCl solution according to the methods described by Shvarov and Bastrakov (1999); these parameters are representative of fluid in equilibrium with the rock, as confirmed by the correct positioning of the Mount Angelay monzonite fluid on the two-feldspar line shown in Figure 14; however, lack of a paragonite-muscovite solid-solution model inhibits calculations of $m_{Na(aq)}$ for rock [5] so the value shown (§) is approximate; MA = Mt. Angelay; - = below detection limit

chemistry was derived, at least in part, by fluid immiscibility; and (3) the complexity of the fluid inclusion populations in any one sample, requiring an assumption as to which fluid could possibly relate to a given alteration assemblage.

Despite the uncertainties, we have compared conventional and microanalytical (PIXE) fluid inclusion results (Mark et al., 2000; Williams et al., 2001) with the geochemical models and have utilized some preliminary PIXE results from Mount Angelay quartz monzonite and pegmatite and from regional albitites. In the albitites, complex NaCl-KCl-$CaCl_2$-H_2O-CO_2 ± hematite-gypsum fluids with two or more daughter minerals and estimated salinity >50 wt percent NaCl equiv are found with relatively simple NaCl-H_2O-CO_2 inclusions of ca. 20 to 30 wt percent NaCl equiv containing only halite as a daughter mineral and with rare mixed CO_2-H_2O-NaCl ± nahcolite inclusions at the Knobby and Tribulation Quarries (de-Jong and Williams, 1995; Oliver, 1995; Fu et al., 2003). CO_2-rich inclusions are also prominent (Table 3). These inclusion types are generally similar to those observed in quartz grains, veins, and pegmatites at the top of the Williams batholith intrusions (e.g., Perring et al., 2000). Complex fluid inclusion chemistry is also evident in iron oxide-Cu-Au deposits of the district (Table 2; see also Williams et al., 2001). Three main inclusion types are found in the ores that correlate generally with those in the albitite-related veins (hypersaline brine, brine, and CO_2-rich fluid), although the hypersaline variety tends to be more chemically complex in the ore deposits than in the albitites.

The inferred (pressure corrected) entrapment temperatures of inclusions associated both with albitites and with the ores are 300° to 550°C and are comparable to the temperatures inferred from mineral assemblages (Table 3). Pressures estimated from CO_2 fluid inclusion densities range from 150 to 400 MPa for the deposits and the albitites (e.g., Mark et al., 2000; Fu et al., 2003). The highest homogenization temperatures and CO_2 densities for individual samples suggest primary fluid entrapment at 400° to 550°C and 300 to 400 MPa, consistent with the alteration assemblages developed (Tables 2, 3). Using starting model conditions of 530° to 550°C and 350 MPa, consistent with the hottest and deepest parts of the system (e.g., Fig. 2, Table 3), we chose three possible starting fluid compositions (Table 7): (1) in equilibrium with Mount Angelay two-feldspar quartz monzonite; (2) a somewhat arbitrary composition similar to (1) but having a slightly elevated Na/K ratio just inside the albite-stable field; and (3) with its starting Na/K ratio increased to match the calculated Na/K ratio determined from fluid inclusions within quartz grains in the quartz monzonite.

Model fluid in equilibrium with the two-feldspar quartz monzonite at the top of the Mount Angelay pluton was calculated by titrating an excess of that rock into a simple $3m_{HCl}$ fluid (similar calculations were performed on the calc-silicate and pelitic rocks to determine the background composition of fluids buffered by these rock types; Table 6). The calculation then partitions the chlorine into molecular and dissociated species in fluid in equilibrium with a subsolidus granitoid. A realistic pH (5.1), a mineral assemblage that remains the same as in the input (i.e., the system is rock buffered), and a calculated Na/K ratio that is consistent with previously published studies of albite-K-feldspar equilibrium (Table 7, Fig. 14) are positive encouragement that the calculations are valid. The relatively high Na/K ratio observed in the actual fluid inclusions could reflect a number of different processes (see below). Our three chosen model fluids have Na/K ratios that range between this theoretically determined fluid (in equilibrium with two feldspars) and the Na/K ratio determined from the fluid inclusion analysis. This range of model fluid inputs then provides some permissive tests of whether granite-derived fluids could have caused bulk albitization of the wall rocks, notwithstanding the many uncertainties associated with the assumption of simple activity-composition relationships in hypersaline brines. We also needed to make the model fluids more dilute than the fluid inclusions to avoid problems of uncertainty in extrapolation of the extended Debye-Hückel equations to high salinity at high T and P. Finally, we added some sulfur species (0.001 m each of H_2S and SO_4) to approximate conditions near hematite-magnetite-pyrite even though these sulfur species were not readily detectable in the fluid inclusions.

Results

Figure 15 shows the results of the simple isothermal fluid/rock mixing models for calc-silicate rocks from Mount Angelay and for the Snake Creek pelites, the two rocks most representative of metasedimentary precursors to albitization. When we used the model fluid initially in equilibrium with two-feldspar quartz monzonite (fluid [1]), alteration assemblages in the pelites generally did not match those observed in the field. A reaction of the same fluid with Mount Angelay calc-silicate rocks results in a quartz-rich alteration at the highest fluid/rock ratios, which precedes an albite-rich assemblage with lesser quartz, biotite, actinolite, clinopyroxene,

TABLE 7. Compositions of Calculated Input Fluids and Comparison with PIXE Data from Fluid Inclusions

	Calculated compositions using HCh software				PIXE data from fluid inclusions						
	[1] Mt Angelay two-feldspar fluid 1	[2] Mt Angelay adjusted fluid 2	[3] Mt Angelay adjusted fluid 3	Output fluid after alteration of calc-silicates	Mt. Angelay monzonite mean (3)	Mt. Angelay pegmatite mean (12)	Regional albitite mean (7)	Starra ironstone mean (6)	Starra ore mean (8)	Eloise ore mean (2)	Ernest Henry Gt stage 3444
Log Na/K (total)	0.48	0.64	1.43	0.88	1.43	0.95	0.66	0.69	0.72	0.60	0.72
Log Na/Fe	2.63	2.66	2.74	1.75	1.68	1.36	1.34	0.48	0.82	0.73	0.48
Log Ca/Fe	0.29	0.29	0.29	0.20	1.01	0.40	0.61	–0.42	0.51	0.52	–0.39
Log Na^+/K^+	0.33	0.50	1.32	0.73							
H^+	1.90E–05	2.40E–05	2.01E–05	4.87E–05							
K^+	4.63E–01	3.45E–01	6.26E–02	2.10E–01							
Na+	9.92E–01	1.09E+00	1.31E+00	1.17E+00							
log K^+/H^+	4.39	4.16	3.49	3.64							
log Na^+/H^+	4.72	4.66	4.81	4.38							
pH	5.23	5.13	5.20	4.83							
$\log f_{O_2}$	–19.9	–19.8	–18.9	–20.0							
H_2O (g)	1000	1000	1000	1000							
Ca (mol)	1.01E–02	1.01E–02	1.01E–02	2.81E–02	1.30E+00	5.95E–01	1.12E+00	5.49E–01	1.55E+00	1.64E+00	4.94E–01
Cl (mol)	2.96E+00	2.96E+00	2.96E+00	2.90E+00	9.38E+00	8.11E+00	1.04E+01	9.62E+00	9.33E+00	8.53E+00	1.08E+01
Fe (mol)	5.17E–03	5.17E–03	5.17E–03	4.47E–02	1.27E–01	2.39E–01	2.76E–01	1.43E+00	4.84E–01	5.01E–01	1.20E+00
K (mol)	7.35E–01	5.44E–01	9.77E–02	3.26E–01	2.26E–01	6.14E–01	1.31E+00	8.83E–01	6.04E–01	6.89E–01	6.86E–01
Na (mol)	2.20E+00	2.39E+00	2.84E+00	2.49E+00	6.08E+00	5.50E+00	6.00E+00	4.30E+00	3.17E+00	2.72E+00	3.62E+00
Mg (mol)	1.07E–04	1.07E–04	1.07E–04	8.30E–04							
Al (mol)	3.09E–04	2.94E–04	3.09E–04	2.52E–04							
Si (mol)	1.29E–01	1.28E–01	1.29E–01	1.28E–01							
H (mol)	5.16E–01	5.18E–01	5.16E–01	5.72E–01							
O (mol)	5.16E–01	5.16E–01	5.16E–01	5.19E–01							
CH_4 (mol)				6.86E–12							
CO_2 (mol)				3.20E–03							
H_2S (mol)	1.00E–04	1.00E–04	1.00E–04	1.81E–04							
SO_4 (mol)	1.00E–04	1.00E–04	1.00E–04	1.18E–05							

Notes: Fluids in the first three columns were calculated using the methods described in the text and figures; data is reported as molal or molal ratios for the calculated data and as moles determined by direct recalculation for the PIXE data (see also Fig. 17); locations are shown in Figure 1; the fourth column is model effluent fluid from reaction of fluid [3] with Mt. Angelay calc-silicate rock during albitization (Figs. 15, 16); PIXE data were gathered according to the methods outlined by Ryan et al. (1995); PIXE data are from Williams et al. (1999, 2001), Mark et al. (2000), Fu et al. (2003), and the Mt. Angelay data are from G. Mark (unpub. data)

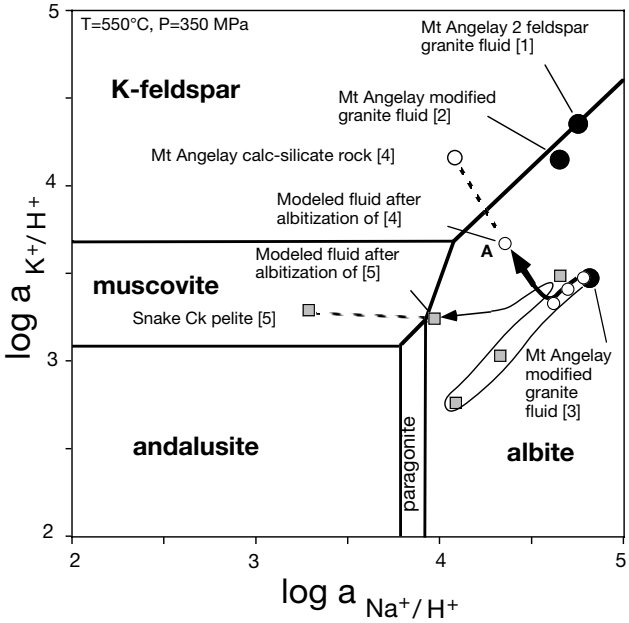

FIG. 14. Na-K activity-activity diagram, constructed for the P-T conditions indicated using the ACT2 module of The Geochemists Workbench (version 4.0.2, Bethke, 2002) and a revised thermodynamic dataset derived from the UNITHERM database of HCh, using the UT2K and K2GWB utilities of Cleverley and Bastrakov (unpub. data). The three starting fluids are shown as heavy dots ([1], [2] and [3]). The compositions of fluid in initial equilibrium with Mount Angelay two-feldpsar quartz monzonite [1], Snake Creek pelite [4], and Mount Angelay calc-silicate rock [5] were calculated by model equilibration of a small amount of dilute HCl solution with an excess of rock as described in the text. Modified initial fluid [3] was calculated by adjusting the Na/K ratio of fluid [1] to match the fluid inclusion data, and fluid [2] is an arbitrary mixture of 10 percent of fluid [3] with fluid [1]. The paths indicated represent the shift in the Na^+/K^+ ratio of the modified Mount Angelay fluid [3] during albitization of Mount Angelay calc-silicate (heavy arrow, open circles) and Snake Creek pelite (light arrow, shaded squares), corresponding to the fluid outputs shown in Figure 16e and f. Molality ratios from HCh output are equated to activity ratios in this diagram with the assumption that the activity coefficients cancel out. However, the diagram is constructed for $a_{H_2O} = 1.0$, which is the main reason the andalusite-bearing Snake Creek pelite plots in the muscovite field instead of on the muscovite-andalusite boundary. The condition of $a_{H_2O} = 1.0$ is not sustained during the model runs due in part to fluid interaction with rocks containing volatile-bearing phases.

epidote, and magnetite, followed at low fluid/rock ratios by assemblages similar to those of the least altered rocks observed in the field (biotite-K-feldspar-quartz-clinopyroxene and plagioclase). Plagioclase of An_{60} is an approximation to mizzonitic (calcic) scapolite found in the actual rock, for which no thermodynamic data are available in the version of UNITHERM we used. The albite-rich alteration assemblage is not entirely unrealistic; however, the anorthite content of the model plagioclase is high relative to that observed in the field (An_{10}-An_{20} instead of An_1-An_{11}), and biotite is still preserved in the model rocks whereas it is usually absent in strongly albitized calc-silicate rocks in the field. Nevertheless, because the fluid Na/K ratio of a two-feldspar granitoid is initially higher than that in equilibrium with a K-feldspar + biotite-bearing scapolitic calc-silicate rock (Fig. 14), the albite alteration predicted in this model is consistent with the field data.

In the simple fluid/rock mixing models, use of fluids [2] and [3] with the Na/K set to values higher than for fluids in equilibrium with two-feldspar granite, produces more realistic alteration assemblages. Using the slightly modified fluid [2] interacting with the pelite, albite-rich alteration with accessory biotite is the outcome of high fluid/rock ratio models, and at a moderate fluid/rock ratio an albite-biotite-rutile-muscovite assemblage is produced. These assemblages are observed in the field, although it is rare for muscovite to be stable together with albite, and biotite is normally destroyed in the most albitized rocks, with rutile stable instead (Rubenach and Lewthwaite, 2002). Using fluid [3], with the Na/K set to that of the Mount Angelay fluid inclusions produces an albite-actinolite-titanite assemblage at a high fluid/rock ratio, and interesting albite-talc-chlorite-paragonite-rutile assemblages at a moderate fluid/rock ratio. Talc is not observed in the field, however cordierite and orthoamphiboles are locally found together with chlorite in albite alteration zones. The version of UNITHERM we used in the calculations does not contain cordierite because of incompatibilities with some of the modified data for iron (Shock et al., 1997), a problem we are resolving currently. We regard the albite-talc-chlorite assemblage as equivalent to the albite-chlorite-orthoamphibole-cordierite assemblage observed in the field. Actinolite and titanite are found in some extremely albitized pelitic rocks. Both fluids [2] and [3] interacting with Mount Angelay calc-silicate rock produce very realistic alteration assemblages, but these do not differ greatly from that produced by fluid in equilibrium with two-feldspar granite [1]. The main difference is the more realistic destruction of biotite during Na-Ca alteration (albite-actinolite-clinopyroxene-titanite). Running any of these models at lower temperatures for pelites produces much more paragonite, and its absence in the field suggests that, at least in the Snake Creek location, alteration occurred at high temperatures.

In the more realistic reactor-type models (Fig. 13b), isothermal infiltration of fluid equilibrated with two-feldspar granite [1] into pelites produces broad albite-K-feldspar alteration zones in which biotite remains stable and muscovite also remains stable closer to the pseudofront (Fig. 16a). This alteration is not observed in the field. Reaction of the same fluid with the calc-silicate rock, however, produces very interesting assemblages (Fig. 16b). Closest to the pseudofront a realistic assemblage of albite-actinolite-quartz-magnetite is produced, with biotite remaining stable but less abundant than in the unaltered rock ahead of the pseudofront. A reaction front is observed in the proximal part of the system in which K-feldspar and clinopyroxene dominate over albite and actinolite. In the field, K-feldspar-clinopyroxene skarns are common in close proximity to the granitoids, so overall, this model, using granite-equilibrated fluids, produces quite realistic results.

If the modified input fluids [2] and [3] are used, albite-rich alteration is prominent in the pelites. Biotite is preserved over larger distances if the only slightly modified fluid [2] is used (Fig. 16c), whereas albite-talc-rutile assemblages are prominent if the Na-rich fluid [3] is used, approximating the cordierite-bearing field assemblages discussed above (Fig. 16e). Paragonite is produced, although it is not observed in the field. The same fluids infiltrating calc-silicate rock produce very realistic alteration assemblages (Fig. 16d, f) in

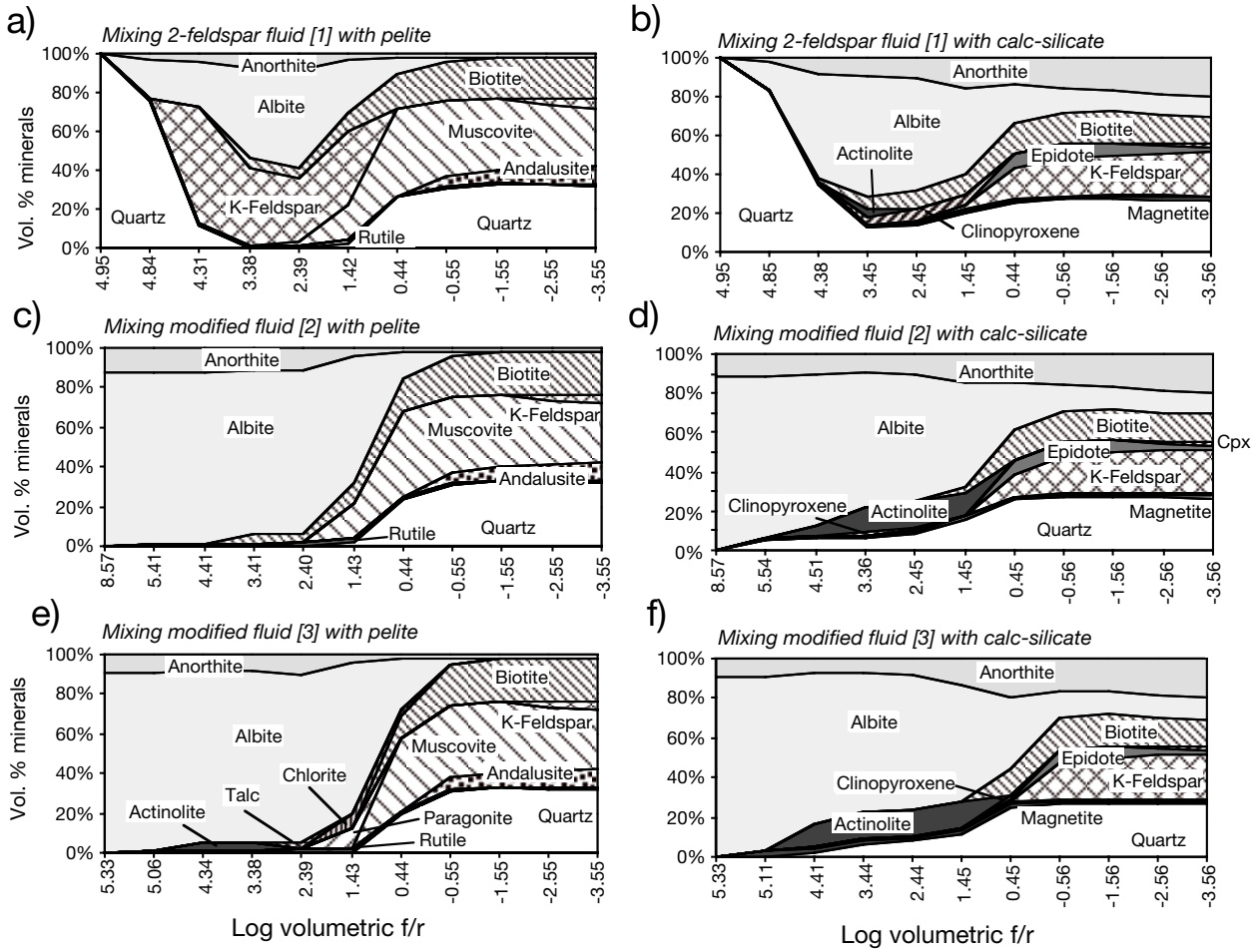

FIG. 15. Simple aliquot-type HCh models of fluid-rock interaction, calculated using the methods described in the text and in Figure 13a. Input rocks and fluids are shown in Tables 6 and 7. (a), (b), and (c) show results from reaction of pelite with the three fluids with different starting Na/K ratios, [1], [2] and [3] in Figure 14. (d), (e), and (f) show results from reaction of calc-silicate rock with the same three fluids. Outputs are in normalized vol percent of minerals; the fluid/rock ratios (f/r) in the individual equilibrations are shown in the bottom axes. Slight variations in these ratios from diagram to diagram are a function of the specific fluid composition chosen and also the loss or gain of volatile-bearing phases in the rock. Predicted assemblages corresponding to each fluid/rock ratio are independent of adjacent calculations, so the bottom axes do not correspond to progressive reaction zones. However, they give some indication of the types of assemblages that may occur from the distal to proximal parts of the hydrothermal system.

which the restricted distribution of biotite in the albite-altered rocks, together with zoning from albite-actinolite to albite-clinopyroxene, are reminiscent of some of the detailed zonation observed in the field (Table 3). However, these models do not reproduce the K-feldspar-clinopyroxene skarns observed close to the granitoids.

To see what effect temperature gradients away from the fluid source may have had, we ran polythermal, polybaric models for reaction with the calc-silicate rock across a range of P-T such that the influx point was still at 550°C and 350 MPa but the limit of infiltration was at 450°C and 250 MPa (Fig. 16g-i). The fluid equilibrated with the two-feldspar granite [1] produced a broad zone of quartz-bearing biotite-K-feldspar alteration with minor magnetite, reminiscent of one of the main alteration stages at Ernest Henry (Fig. 5) but also typical for cooling fluids emanating from granites (e.g., in porphyry systems, Ulrich and Heinrich, 2001). If the starting fluid composition is shifted just into the albite field (fluid [2], Fig. 14), cooling produces voluminous albite with additional actinolite, then biotite and magnetite with increasing distance from the source. Using the most Na rich starting fluid composition [3], quartz-destructive albite-clinopyroxene alteration is followed at lower temperature (and farther from the starting point) by albite-actinolite-quartz and eventually biotite- and chlorite-bearing albite rocks.

Aspects of the fluid evolution through these reactor-type models are also presented (Fig. 16). Notably, in the reaction zones just behind the pseudofront, where albitization is most intense, the locally equilibrated fluid attains high concentrations of components initially absent from the fluid but present in the rock. For the isothermal models, the granite-equilibrated fluid [1] leaches Fe from the pelite and Ca and Fe from the calc-silicate rock, but its Na/K ratio remains nearly constant. The more sodic fluids [2] and [3] strip Fe and K

from the pelite and Fe, K, and Ca from the calc-silicate rock. The latter trends are more consistent with the bulk geochemical changes observed for albitization (Fig. 10). The preliminary PIXE work shows that fluid inclusions in albitized calc-silicate rocks are Ca rich relative to those hosted by pelites (B. Fu et al., unpub. data), suggesting at least some of the chemistry of the fluids was a consequence of partial equilibration with the wall rocks. For reaction with altered calc-silicate rock in a thermal gradient (Fig. 16g-i), both fluids [1] and [2] fail to leach Fe from the rocks, rather they lose iron to the rock via biotite formation and gain substantial Ca. These trends do not match the geochemical patterns for albitization (Fig. 10), although they are interesting in the context of ore-proximal alteration (see below). In contrast, the initially high Na/K fluid [3] leaches a large amount of iron during albitization in the thermal gradient and shows a good match with the alteration geochemistry (Fig. 10) and mineral assemblages developed.

The results of the isothermal models are compared with the compositions of the model input and output fluids in Figure 14. The diagram shows the different starting fluid compositions from equilibrium with the granite ([1]) through to fluids ([2] and [3]) initially in the albite field. For fluid [3], with the Na/K ratio adjusted to that of the Mount Angelay fluid inclusions, the initial path during albitization of calc-silicate rock is along a line of a near-constant Na^+/K^+ ratio but within the albite field, followed by a shift toward more potassic fluid compositions as the effect of the host rock impacts on the fluid chemistry at the head of the infiltration column. For infiltration of this same fluid into the pelites, the fluid follows a convoluted path partly controlled by the stability of the talc and chlorite-bearing assemblages, with fluid just behind the head of the infiltration column being close to the muscovite field (Fig. 16).

Most of the Fe oxide-Cu-Au deposits occur in the Soldiers Cap Group, and those that are hosted in the Mary Kathleen Group are predominantly in siliciclastic or volcanic rocks rather than calc-silicate rocks (e.g., Fig. 2). To test this scenario, we took the effluent fluid from albitized calc-silicate rocks (labeled A, Fig. 14) and reacted that fluid with fresh pelitic rocks at 550°C (Fig. 17). Possible alteration assemblages contain abundant magnetite, clinopyroxene, biotite, and titanite, as well as albite, mimicking many of the alteration styles seen in the near vicinity of the deposits (Table 2). Calcite veins or breccia matrix are common in some of the deposits—if the Ca content of this effluent fluid is lowered to simulate loss of Ca to calcite veins (Fig. 17b), actinolite becomes predominant in the alteration rather than clinopyroxene. Particularly noteworthy in this context are the clinopyroxene-magnetite gangue at Mount Elliott (Little, 1997), some albite-magnetite rocks in the Snake Creek area, the transition from hornblende-magnetite to biotite-chlorite alteration at Eloise (Baker, 1998), and early Na-Ca-Fe alteration (actinolite, clinopyroxene, magnetite) followed by biotite-magnetite-K-feldspar at Ernest Henry (Mark et al., 2000).

Comparison with fluid inclusion data

Figure 18 compares the modeled reaction paths and input compositions with the PIXE data for fluid inclusions summarized (Table 7). Although we have used more dilute model fluids than those indicated from the fluid inclusion data, the model trends are similar to apparent trends in the PIXE results. Hypersaline brines from the deposits and from the albitites appear to have either higher Ca or K concentrations than most of the fluids sampled from the granitoids (Fig. 17a), even though the bulk salinities are similar (Table 6). Using fluid equilibrated with two-feldspar granite [1], the Ca concentration of the fluids increases with alteration although the K concentration is little changed. The more sodic fluids [2] and [3] produce L-shaped trends with initial Ca enrichment followed by K enrichment, and arguably these trends are similar to those for the PIXE data. If the PIXE data are compared, the evolution from granite-derived fluid through to the deposits and regional albitized calc-silicate and pelitic rocks involves a decrease in the molar Na/K ratio of around 0.7 log units. The most comparable shift in Na/K ratio of the fluids from the model runs was attained with fluid [3] (with starting Na/K adjusted to that of the average Mount Angelay quartz monzonite inclusions). Fluids [1] and [2] shift <0.2 log units lower in molar Na/K for albitization of calc-silicate rocks. The Na/K ratio of fluid [1] increases slightly during albitization of pelite, which is inconsistent with the overall fluid inclusion data.

Discussion and Conclusions

The titanite ages for the Cloncurry district suggest a strong temporal relationship between intrusion and albitization, strengthening models that proposed a genetic link (Mark and Foster, 2000; Pollard, 2001). Similarity between the Mary Kathleen fold belt titanite ages and those of the Cloncurry district suggests a widespread 1550 to 1500 Ma Williams batholith-related albitization event (see also Foster and Rubenach, 2000) and may indicate that intrusions of this age lie below the Mary Kathleen fold belt, even though only rare pegmatites of appropriate timing are exposed (Fig. 2) . However, the 1595 Ma ages for albitization at Osborne are much older than the Williams batholith, despite the abundance of pegmatites, which could be a product of local anatectic melting (Rubenach et al., 2001). The 1595 Ma age of the albite alteration requires earlier, unexposed intrusions (linked to the pegmatites?) as causes of albitization or alternative sources for these early albitizing fluids.

The stable isotope data for albitization during the 1550 to 1500 Ma thermal event suggest that a fluid in equilibrium with calcite having $\delta^{18}O$ values of 11.0 per mil and $\delta^{13}C$ values of –6.0 per mil infiltrated the Mary Kathleen and Soldiers Cap Groups at a high temperature. Because the unaltered Corella Formation rocks, so prominent in the regional geology, have a distinctive marine carbonate signature, average crustal equilibrated fluid does not provide the best solution for the stable isotope ratios of calcite in the altered and mineralized rocks. The largest shift from initial marine carbonate isotope signatures occurred in the vicinity of large podiform veins and intensely brecciated and albitized rocks, and the bulk of the variations observed in the C and O isotope data are a consequence of a high-temperature reaction between initial metasediments and an infiltrating fluid that was grossly out of equilibrium with the metacarbonates. The measured values are typical for fluids derived from, or equilibrated with, felsic igneous rocks. The albitites and carbonate veins contain calcite having $\delta^{18}O$ and $\delta^{13}C$ values similar

to the iron oxide-Cu-Au deposits. Together with a predominance of igneous-like S isotope values for sulfides from the deposits and local albitite-related pyrite at Ernest Henry (Mark et al., 2000), these data point toward an igneous fluid source. By inference then, the regional albitization of broadly similar timing to the Williams batholith was most likely produced by fluids derived at least partly from crystallizing plutons (see also Pollard, 2001).

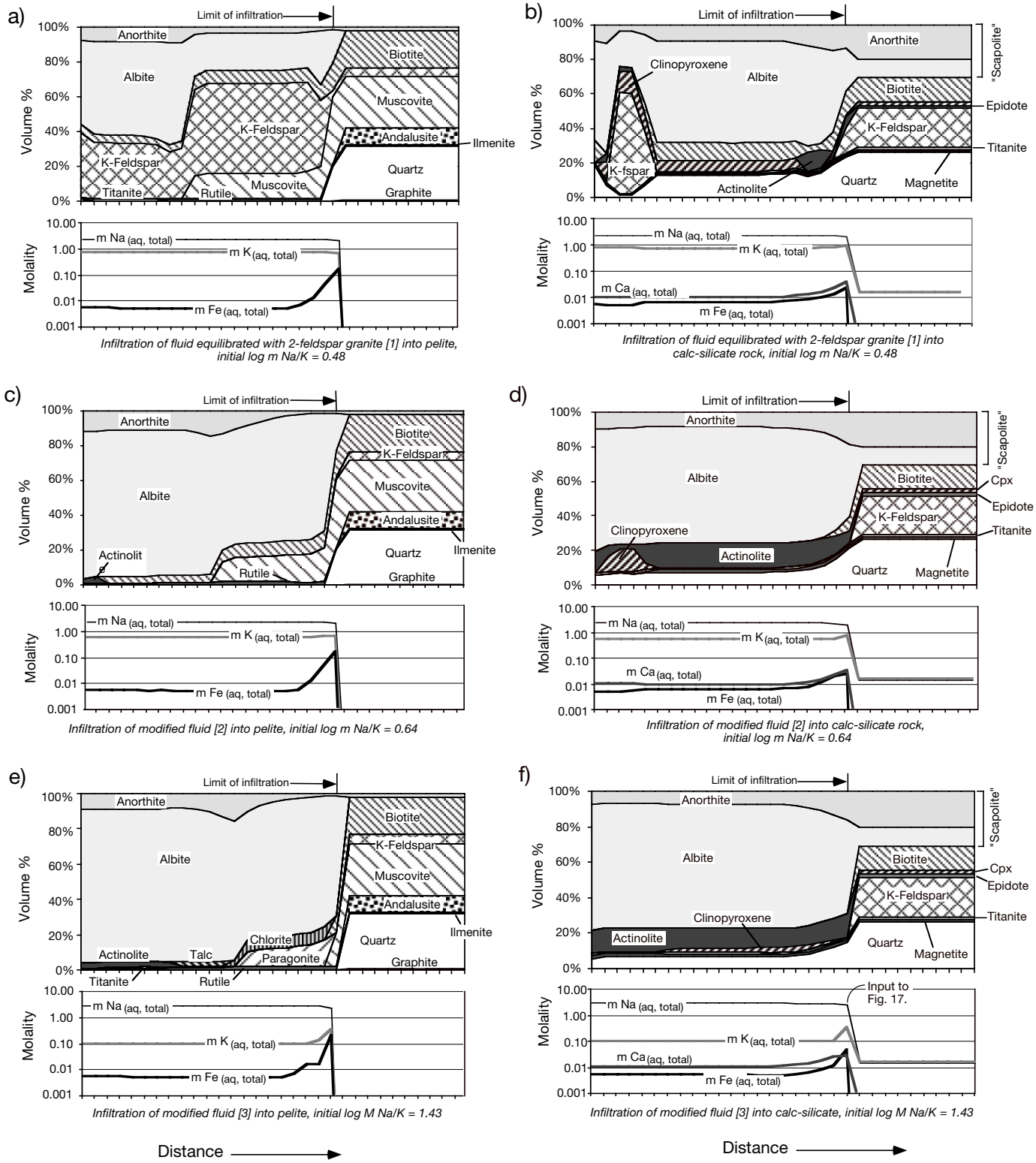

Source of NaCl

Oliver et al. (1993), in their discussion of the calcite veins in the Mary Kathleen fold belt, concluded that the externally derived fluid was of igneous or "average metamorphic" (but noncarbonate) derivation. However, they noted that the intense albitization required highly saline fluids, for which a salt source was not clearly evident in that belt. They appealed to selective dissolution of pure halite layers from the meta-evaporite sequence to explain the high salinities but drew particular attention to the paradox of highly saline fluids and apparently magmatic stable isotope values grossly out of equilibrium with the host metacarbonate-evaporite sequence. After deposition of the Corella Formation (ca. 1750 Ma) and up to and including the Isan orogeny at 1600 Ma, it is possible that production of saline fluids occurred at moderate temperatures by evaporite dissolution (Oliver et al., 1994). This may be an explanation for the high fluid salinities associated with albitites in the ca. 1600 Ma Osborne deposit. However, during the later intrusion of the Williams batholith, saline fluids could no longer have been derived én masse from the Corella Formation meta-evaporites because most of the evaporite salt should have been sequestered into scapolite by the earlier thermal events. Saline pore fluid contained within scapolitic metamorphic rocks (Oliver et al., 1992) may have been liberated during albitization (e.g., by destruction of fluid inclusions and release of other grain boundary fluids). A small amount of NaCl may have been all that was needed to shift the fluids into the albite-stable field (Fig. 14), but the amount of Na actually transferred into the albitized rocks is still extraordinary, and the stable isotope data also require that the bulk of the oxygen and carbon in calcite, at least, was derived from outside the Corella Formation and most likely had an igneous source. An evaporite would have had to be situated in an overlying, unmetamorphosed sequence, which

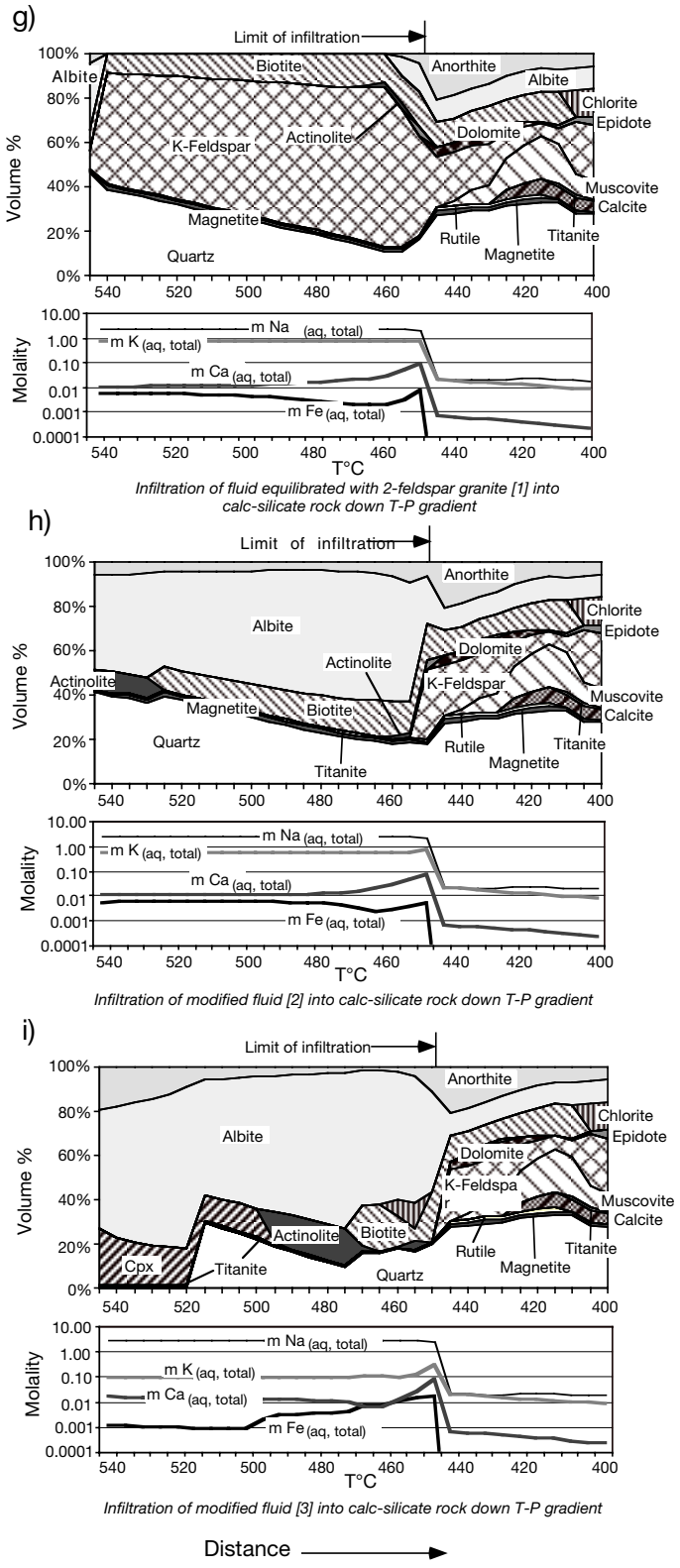

FIG. 16. Reactor-type HCh models portraying progressive infiltration of the same fluids used in Figure 15 (Table 7) through a rock column (rocks in Table 6), according to the methods described in Figure 13b and the text. Fluid of the same composition is added to the input point (left) and, upon completion of each reaction step (ticks on x-axis), is then displaced into the next block of rock by a fresh batch of fluid added to the left (cf. Heinrich et al., 1996). Models (a), (c), and (e) show isothermal infiltration of pelites with the three fluids of different Na/K ratio, as indicated. Models (b), (d), and (f) show isothermal infiltration of calc-silicate rocks with the same three fluids. The real starting rocks contain scapolite, but our version of UNITHERM contained no scapolite data. However, the predicted plagioclase composition (An_{60}) is similar to the equivalent anorthite content in the actual scapolites (Mark, 1998b). Models (g), (h), and (i) show retrograde (down P-T) infiltration of calc-silicate rocks from 550° and 350 to 400°C and 200 MPa, also with the same three starting fluids. The down-temperature variation in assemblages ahead of the limit of infiltration is not relevant to the field situation, as the rocks had already been metamorphosed to at least 450°C prior to the alteration depicted behind the fronts. The bottom half of each part of the diagram shows the calculated molalities of the indicated fluid species. Although no dimensions are shown on the x-axis of each plot, they are interpreted to correspond to the distances indicated for altered versus nonaltered rocks shown in Figures 3 and 4, i.e., kilometer to 10-km scales. However, because we have demonstrated that complex fracture systems hosted the infiltrating fluid (e.g., Oliver et al., 1990; Marshall, 2003), the x-axes could also represent meter-scale variations in alteration assemblage dependent on proximity to fractures, in which case multiple fracturing and wall-rock alteration overlapping in time and space could have produced the 100-m-scale patterns shown in Figures 5 and 6 and ultimately the kilometer-scale patterns shown in Figures 3 and 4. (e) and (f) correspond to the paths shown in Figure 14. The indicated point immediately behind the limit of infiltration in (f) was used as an input fluid to simulate ore-proximal alteration in Figure 17.

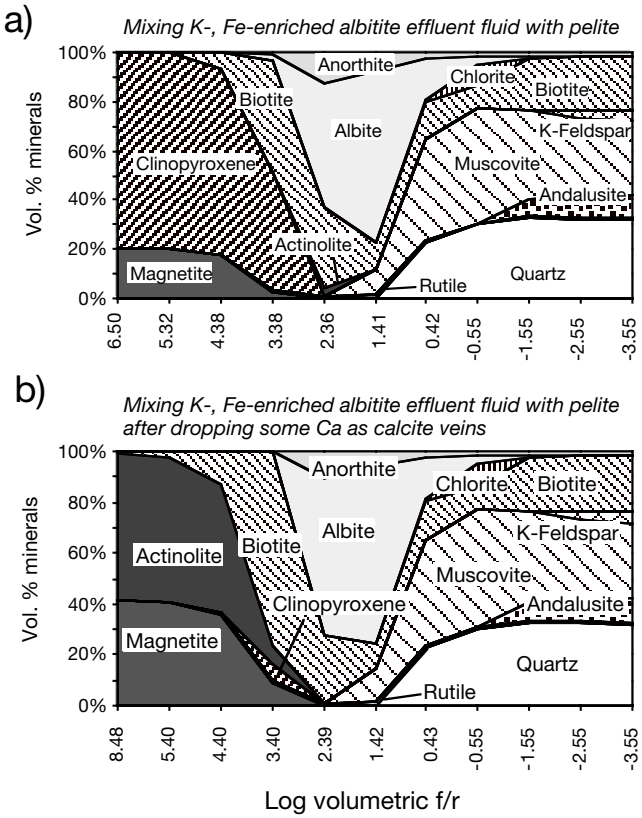

FIG. 17. Aliquot-type HCh models (see Fig. 13a) for reaction of fluid modified by albitization of calc-silicate rocks (see indicated arrow bottom of Fig. 16f and column 4 of data in Table 7) with pelites (Table 6). The models attempt to test the envisaged reaction path of fluids shown in Figure 19 in which albitization of calc-silicate rocks in the lower sequences above the granites and the associated increase in K, Fe, and Ca concentrations in the fluid is a likely precursor to formation of ironstones in the overlying sequence. a. Model based on the output from Figure 16f. b. Model generated by decreasing the $m_{Ca(aq,\,total)}$ artifically from 0.028 to 0.018, with the assumption of Ca loss due to calcite veining. The outputs, particularly on the left side of the diagrams (high f/r), are similar to proximal alteration surrounding several of the deposits, as discussed in the text.

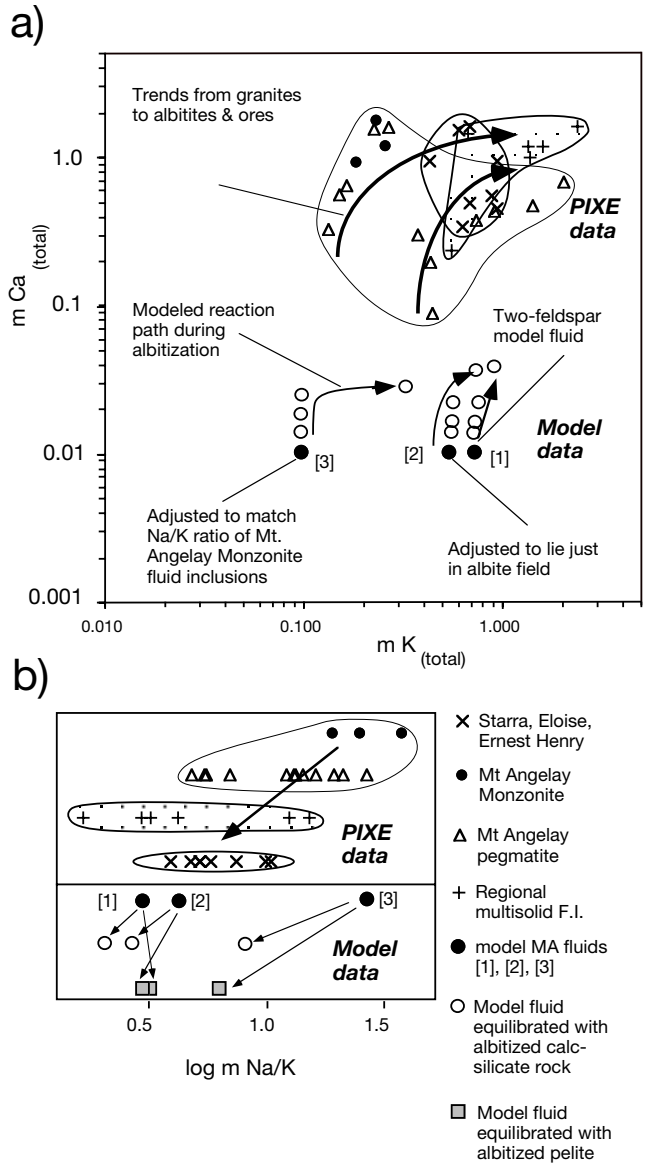

FIG. 18. a. Comparison of raw PIXE K and Ca data from hypersaline fluid inclusions with multiple daughter minerals from the indicated sources (Table 7), with the inputs and outputs to the HCh models described in Figure 16. The model K and Ca contents are much lower than the PIXE data because of the thermodynamic limits of extrapolation of fluid activity-concentration relationships using Debye-Hückel parameters (e.g., Sverjensky et al., 1997). b. Comparison of PIXE Na/K ratios with modeled ratios during albitization depicted in Figure 16. The Na content of the fluid inclusions was determined by charge balance so is subject to substantial errors because of poor precision in Cl determinations (cf. Williams et al., 2001) and uncertainty in speciation. However, the determined Na contents are consistent with the microthermometric fluid inclusion data (Fu et al., 2003). The overall trends toward higher Ca and K contents and lower Na/K ratios from the model albitization (using fluid [3] with Na/K ratios set to match Mount Angelay monzonite fluid inclusions) generally match the trends inferred from the fluid inclusion data from proximal (granites) to distal (albitites, orebodies). See text for further discussion.

would have required either exhumation of the sequence immediately after the 1600 Ma metamorphism or the downward penetration of surface evaporite-derived fluids into the belt during exhumation. Penetration of near-surface fluids deep into mountain ranges such as the Isan orogenic belt has been proposed elsewhere (Wickham and Taylor, 1987; Koons and Craw, 1991; Jenkin et al., 1994), but typically such topographically or mechanically driven fluid flow is incapable of penetrating more than 5 or 8 km. Some of the fluid inclusion data would permit low-pressure exhumation interpretations (130–150 MPa), but CO_2 density data for fluid inclusions in the ore deposits gives pressures in excess of 300 MPa, making it less likely that surface-derived evaporite fluids could have been involved.

A more likely source for most of the salt that caused post-peak metamorphic albitization was from the crystallization of the Williams Suite intrusions (Fig. 19). Pollard (2001) proposed a model whereby immiscible separation of a complex $NaCl\text{-}H_2O\text{-}CO_2 \pm CaCl_2$ fluid into a hypersaline brine and a CO_2-rich gas resulted in a hydrothermal fluid that would have been in equilibrium with albite at high temperatures above the pluton. He also estimated that the total Na budget accompanying albitization could be achieved by release of magmatic fluids given the wide extent of the Williams Suite (Fig.

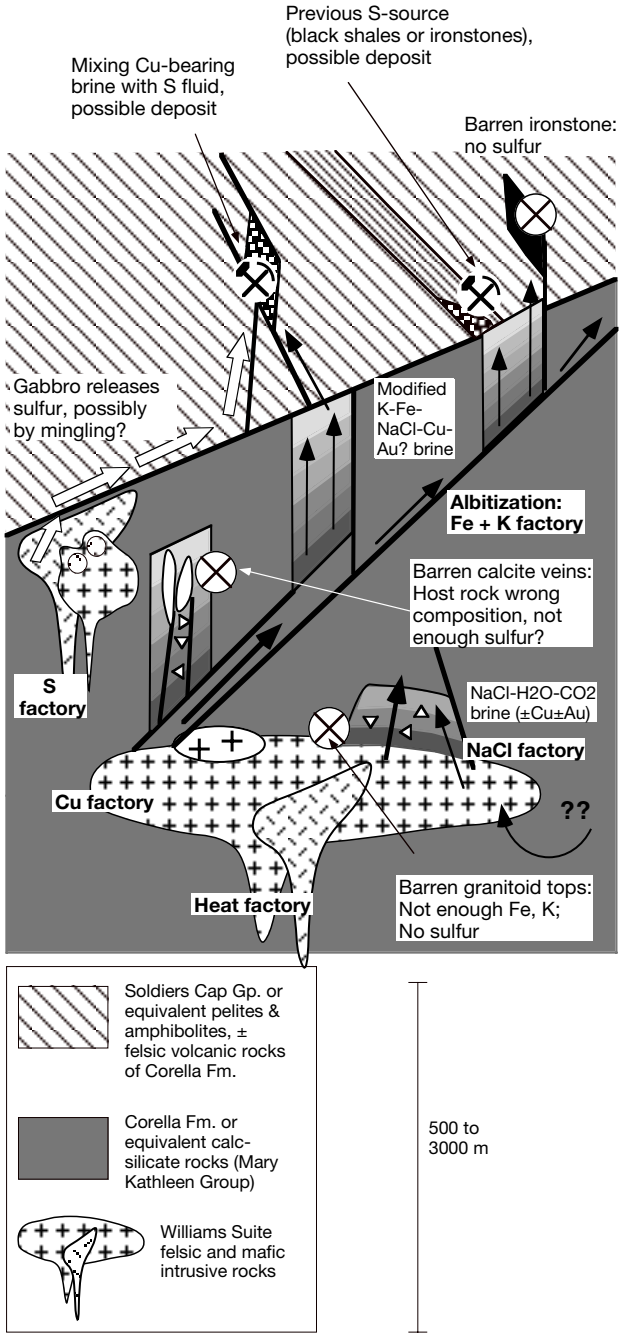

FIG. 19. Cartoon cross section explaining the distribution and generation of albitites and the likely chemical reaction paths between source rocks, albitites, and ore deposits of the Eastern Succession. Black arrows are inferred pathways of brines, white arrows are speculated sulfur-bearing fluids. Optimal conditions for ore genesis require a previous history of fluid modification via albitization (variable gray shading), a structural trap, a reactive host rock in overlying schists (or noncalc-silicate rocks of the Mary Kathleen Group), and a sulfur source, as indicated. Barren ironstones may be produced via the modeled albitization path but lack sulfur. All pyrite-magnetite ironstones contain chalcopyrite, so the availability of Cu is not a limiting factor. For at least some of the deposits a likely origin for sulfur from crystallizing or leached gabbros (or possibly even mantle-derived fluids) is constrained by $\delta^{34}S$ values of sulfides from the deposits near 0 per mil (Mark et al., 2000; Baker et al., 2001). Also, although our data strongly support a major magmatic component to the alteration and mineralization (including Cu), we have not completely excluded possibilities of exotic NaCl replenishment (see also Williams et al., 2001).

2). Albitization by magmatic fluids has been observed for some two-feldspar granites and pegmatites elsewhere (e.g., Charoy and Pollard, 1989). Relative to H_2O-NaCl fluids, albite is preferentially stabilized over K-feldspar in the presence of elevated CO_2 (Iiyama, 1965), and this is the basis for shifting our preferred model albitizing fluid to a higher Na/K ratio than fluid in equilibrium with two-feldspar granite. The widespread abundance of albite in the Eastern Succession alteration systems, predominant over K-feldspar, is interpreted to reflect periodic replenishment of NaCl but also the contribution of CO_2 released by both magma crystallization and by wall-rock alteration of carbonates.

Relationship to mineralization

Geochemical data indicate that the albitization process added Na to the rocks and released Fe, K, Ba, Rb ± Ca, Sr, Co, V, Mn, Pb, and Zn to the fluid. The leached elements are those that are specifically enriched in the proximal biotite-magnetite alteration zones of the Cu-Au ore deposits (Fig. 9g), although Fe and K are also found in barren ironstones and biotite-rich alteration in Snake Creek rocks (Rubenach and Lewthwaite, 2002). In the case of Pb and Zn (which we have not modeled), the loss of these components is apparently matched by their enrichment in ore-related fluid inclusions (e.g., Williams et al., 2001). The geochemical modeling (1) is consistent with the progressive enrichment of Fe and K in the fluid during albitization, (2) demonstrates that the Fe and K concentrations are close to that observed in equilibrium with magnetite and biotite in some of the Cu-Au deposits, and (3) adequately predicts the mineralogy of ore-proximal alteration zones formed in pelites from fluids that had previously albitized calc-silicate rocks (Table 6, Figs. 17, 18). Although the best albitization model results are produced with fluid having an initially elevated Na/K ratio, even fluids equilibrated with two-feldspar granites produce albitites under isothermal conditions and leach iron from calc-silicate rocks. With decreasing P and T during infiltration, albitization is still predicted, and there is a large amount of iron liberated during albitization of calc-silicate rocks.

Our model of fluid infiltration through calc-silicate rock in a thermal gradient using fluids equilibrated with two-feldspar granite produces biotite-K-feldspar alteration similar to that seen around some of the deposits. However, the small amount of magnetite precipitated during such model alteration, and the observation that the deposits are not generally hosted in calc-silicate rocks, precludes a simple conclusion that down-temperature infiltration can produce the ore-proximal alteration. Ongoing modeling is concerned with a range of deposit-forming scenarios other than the ones described here.

The pattern for Cu during albitization remains unclear, and our geochemical data for albitization show no consistent patterns for Cu mobility, despite consistent transfer of Pb and Zn from the rock to the fluid. This could mean that the source of the copper for the deposits may have been from outside the metasedimentary sequence, possibly the Williams Suite for at least the young albitites and ore deposits (Fig. 18). Barren ironstones may have been produced when albitizing fluids were initially poor in Cu, or S, or both. Given the alteration path suggested here for albitization, it is possible that the

chalcopyrite only became saturated in the albitizing fluids upon mixing with S-bearing wall rocks or fluids. Mixing of Cu-bearing fluids with a more juvenile magmatic fluid containing sulfur, or fluid equilibrated with sulfide-bearing mafic rocks, may be required to explain the large tonnage magnetite-chalcopyrite deposits of the district, particularly Ernest Henry. Similarly, strong Ba depletion during albitization requires low sulfate concentrations in the fluid, and mixing to produce barite has apparently occurred only at the sites of known Cu-Au mineralization (Tables 2, 3). Some mineralized ironstones in the Cloncurry district may have depended on S-rich fluids reacting with earlier ironstone rocks (e.g., Rotherham et al., 1998). However, we propose that ore formation mostly occurred by mixing between magmatic S-bearing fluids and saline brines, the latter probably initially of igneous derivation, that were extensively modified by wall-rock interaction which caused the albitization described here.

Acknowledgments

Our thanks to Evgeniy Bastrakov (Geoscience Australia), who introduced us to the HCh software and provided some training, the Geoscience Australia version of the UNITHERM database, and his working files for initial setting of the modeling problem. This research has been conducted through the support of the Australian Research Council (1998–2002), the Australian Minerals Industry Research Association (1993–1997), and the Predictive Minerals Discovery Cooperative Research Centre (2001–2002), the latter two both representing a consortium of mining companies and research groups. Geoscience Australia (then Bureau of Mineral Resources) provided logistical support for earlier fieldwork in the 1980s. Mount Isa Mines Exploration (now XStrata) and James Cook University also provided research support, particularly through the contribution of MIM and Ernest Henry Mines through an Australian Research Council-Special Projects Industry Research and Training (ARC-SPIRT) project to Williams and Oliver at Ernest Henry. Alexander (Sasha) Nemchin at Curtin University (now with Western Australia School of Mines) is thanked for the wet chemistry and mass spectrometry for the titanite U-Pb analyses, Ian Cartwright at the Monash University Stable Isotope Facility is thanked for the carbonate stable isotope results, Mary Yeh helped with geochemical data compilation, and the staff of the Advanced Analytical Centre at James Cook University assisted with geochemical analyses. We acknowledge fruitful discussions with Mark Barton, Mick Carew, Ian Cartwright, Dave Cooke, Richard Crookes, Garry Davidson, Paul Gow, Caroline Perring, Neil Phillips, Chris Salt, Max Tuesley, Rick Valenta, Vic Wall, Steve Walters, Andy Wilde, Dugi Wilson, and Bruce Yardley. John Walshe and Roger Skirrow are thanked for their critical but positive reviews which greatly helped improve the manuscript. Mark Hannington is also thanked for his dedication to the editing task.

December 5, 2002; February 24, 2004

REFERENCES

Adshead, N.D., Voulgaris, P., and Muscio, V.N., 1998, Osborne copper-gold deposit: Geology of the Osborne copper-gold deposit: Australasian Institute of Mining and Metallurgy, v. 22, p. 793–799.

Baker, T., 1996, The geology and genesis of the Eloise Cu-Au deposit, Cloncurry district, NW Queensland, Australia: Unpublished Ph.D. thesis, Townsville, James Cook University of North Queensland, 303 p.

——1998, Alteration, mineralization, and fluid evolution at the Eloise Cu-Au deposit, Cloncurry district, NW Queensland: Economic Geology, v. 93, p. 1213–1236.

Baker, T., and Laing, W.P., 1998, Eloise Cu-Au deposit, east Mount Isa block: Structural environment and structural controls on ore: Australian Journal of Earth Sciences, v. 45, p. 429–444.

Baker, T., Perkins, C., Blake, K.L., and Williams, P.J., 2001, Radiogenic and stable isotope constraints on the genesis of the Eloise Cu-Au deposit, Cloncurry district, northwest Queensland: Economic Geology, v. 96, p. 723–742.

Barton, M.D., and Johnson, D.A., 1996, Evaporitic source model for igneous-related Fe oxide-(REE-Cu-Au-U) mineralization: Geology, v. 24, p. 259–262.

Berman, R.G., 1988, Internally-consistent thermodynamic data for minerals in the system Na_2O-K_2O-CaO-MgO-FeO-Fe_2O_3-Al_2O_3-SiO_2-TiO_2-H_2O-CO_2: Journal of Petrology, v. 29, p. 445–522.

Bethke, C.M., 2002, The geochemists workbench, version 4.0.2: A users guide: Urbana-Champaign, University of Illinois, 224 p.

Bird, D.K., Schiffman, P., Elders, W.A., Williams, A.E., and McDowell, S.D., 1984, Calc-silicate mineralization in active geothermal systems: Economic Geology, v. 79, p. 671–695.

Blattner, P., and Lassey, K.R., 1990, Transport of stable isotopes, kinetics, dispersive advection and the "isotopic fronts" of Baumgartner and Rumble (1988): Contributions to Mineralogy and Petrology, v. 105, p. 486–490.

Borisov, M.V., and Shvarov, Y.V., 1998, Mobilization of ore components during the formation of Pb-Zn hydrothermal lodes: Geochemistry International, v. 36, p. 134–149.

Cartwright, I., 1997, Permeability generation and resetting of tracers during metamorphic fluid flow: Implications for advection-dispersion models: Contributions to Mineralogy and Petrology, v. 129, p. 198–208.

Charoy, B., and Pollard, P.J., 1989, Albite-rich, silica-depleted metasomatic rocks at Emuford, northeast Queensland: Mineralogical, geochemical, and fluid inclusion constraints on hydrothermal evolution and tin mineralization: Economic Geology, v. 84, p. 1850–1874.

Cline, J.S., and Bodnar, R.J., 1991, Can economic porphyry copper mineralization be generated by a typical calc-alkaline melt?: Journal of Geophysical Research, v. 96, p. 8113–8126.

Cook, N.D.J., and Ashley, P.M., 1992, Meta-evaporite sequence, exhalative chemical sediments and associated rocks in the Proterozoic Willyama Supergroup, South Australia: Implications for metallogenesis: Precambrian Research, v. 56, p. 211–226.

Cooke, D.R., and McPhail, D.C., 2001. Epithermal Au-Ag-Te mineralization, Acupan, Baguio district, Philippines: Numerical simulations of mineral deposition: Economic Geology, v. 96, p. 109–132.

Davidson, G.J., and Dixon, G.H., 1992, Two sulphur isotope provinces deduced from ores in the Mount Isa Eastern Succession, Australia: Mineralium Deposita, v. 27, p. 30–41.

Davis, B.K., Pollard, P.J., Lally, J.H., McNaughton, N.J., Blake, K., and Williams, P.J., 2001, Deformation history of the Naraku batholith, Mount Isa inlier, Australia: Implications for pluton ages and geometries from structural studies of the Dipvale Granodiorite and Levian Granite: Australian Journal of Earth Sciences, v. 48, p. 131–150.

deJong, G., and Williams, P.J., 1995, Giant metasomatic system formed during exhumation of mid-crustal Proterozoic rocks in the vicinity of the Cloncurry fault, northwest Queensland: Australian Journal of Earth Sciences, v. 42, p. 281–290.

Dipple, G.M., and Ferry, J.M., 1992, Metasomatism and fluid flow in ductile fault zones: Contributions to Mineralogy and Petrology, v. 112, p. 149–164.

Ferry, J.M., and Dipple, G.M., 1991, Fluid flow, mineral reactions, and metasomatism: Geology, v. 19, p. 211–214.

Foster, D.R.W., and Rubenach, M.J., 2000, Comment: High radiogenic heat-producing granites and metamorphism—an example from the western Mount Isa inlier, Australia: Geology, v. 28, p. 671.

Friedman, I., and O'Neil, J.R., 1977, Compilation of stable isotope fractionation factors of geochemical interest: U.S. Geological Survey Professional Paper 440-KK, 12 p.

Frietsch, R., Tuisku, P., Martinsson, O.L., and Perdahl, J.-A., 1997, Early Proterozoic Cu-(Au) and Fe ore deposits associated with regional Na-Cl metasomatism in northern Fennoscandia: Ore Geology Reviews, v. 12, p. 1–34.

Frost, B.R., Chamberlain, K.R., and Schumacher, J.C., 2000, Sphene (titanite): Phase relations and role as a geochronometer: Chemical Geology, v. 172, p. 131–148.

Fu, B., Williams, P.J., Oliver, N.H.S., Dong, G., Pollard, P.J., and Mark, G., 2003, Fluid mixing versus unmixing as an ore-forming process in the Cloncurry Fe-oxide-Cu-Au district, NW Queensland, Australia: Evidence from fluid inclusions: Journal of Geochemical Exploration, v. 78–79, p. 617–622.

Gauthier, L., Hall, G., Stein, H., and Schaltegger, U., 2001, The Osborne deposit, Cloncurry district: A 1595 Ma Cu-Au skarn deposit [ext. abs.]: Townsville, Australia, James Cook University, School of Earth Sciences, Economic Geology Research Unit Contribution, v. 59, p. 58–59.

Giles, D., and Nutman, A.P., 2002, SHRIMP U-Pb monazite dating of 1600–1580 Ma amphibolite facies metamorphism in the southeastern Mount Isa block, Australia: Australian Journal of Earth Sciences, v. 49, p. 455–466.

Grant, J.A., 1986, The isocon diagram—a simple solution to Gresens equation for metasomatic alteration: Economic Geology, v. 81, p. 1976–1982.

Hand, M., and Rubatto, D., 2002, The scale of the thermal problem in the Mount Isa inlier [abs]: Geological Society of Australia Abstracts, v. 67, p. 173.

Haynes, D.W., 2000, Iron oxide copper (-gold) deposits: Their position in the ore deposit spectrum, *in* Porter, T.M., ed., Hydrothermal iron oxide copper-gold and related deposits: A global perspective: Adelaide, Australian Mineral Foundation, p. 71–90.

Heinrich, C.A., Bain, J.H.C., Mernagh, T.P., Wyborn, L.A.I., Andrew, A.S., and Waring, C.L., 1995, Fluid and mass transfer during metabasalt alteration and copper mineralization at Mount Isa, Australia: Economic Geology, v. 90, p. 705–730.

Heinrich, C.A., Walshe, J.L., and Harrold, B.P., 1996, Chemical mass transfer of ore-forming hydrothermal systems: Current practise and problems: Ore Geology Reviews, v. 10, p. 319–338.

Hitzman, M.W., Oreskes, N., and Einaudi, M.T., 1992, Geological characteristics and tectonic setting of Proterozoic iron oxide (Cu-U-Au-REE) deposits: Precambrian Research, v. 58, p. 241–287.

Iiyama, J.T., 1965, Influence des anions sur les équilibres d'échange d'ions Na-K dans les feldspaths alcalins à 600°C sous une pression de 1000 bars: Bulletin de Societe françois Minéralogie et Cristallographie, v. 88, p. 618–622.

Ito, E., Harris, D.M., and Anderson, A.T.J., 1983, Alteration of oceanic crust and geologic cycling of chlorine and water: Geochimica et Cosmochimica Acta, v. 47, p. 1613–1624.

Jenkin, G.R.T., Craw, D., and Fallick, A.E. 1994, Stable isotopic and fluid inclusion evidence for meteoric fluid penetration into an active mountain belt, Alpine schist, New Zealand: Journal of Metamorphic Geology, v. 12, p. 429–444.

Koons, P.O., and Craw, D., 1991, Evolution of fluid driving forces and composition within collisional orogens: Geophysical Research Letters, v. 18, p. 935–938.

Korzhinskii, D.S., 1970, Theory of metasomatic zoning: London, Oxford University Press, 162 p.

Laing, W.P., 1998, Structural-metasomatic environment of the East Mount Isa block base-metal-gold province: Australian Journal of Earth Sciences, v. 45, p. 413–428.

Little, G.A., 1997, Structural evolution and paragenesis of alteration and mineralization at Mount Elliott Cu-Au mine, northwest Queensland: Unpublished B.Sc. (Honors) thesis, Townsville, Queensland, James Cook University of North Queensland, 98 p.

Mark, G., 1998a, Albitite formation by selective pervasive sodic alteration of tonalite plutons in the Cloncurry district, NW Queensland: Australian Journal of Earth Sciences, v. 45, p. 765–774.

——1998b, Granites and regional alteration in the Cloncurry district, northwest Queensland, Australia: Unpublished Ph.D. thesis, Townsville, James Cook University of North Queensland, 354 p.

Mark, G., and Foster, D.R.W., 2000, Magmatic-hydrothermal albite-actinolite-apatite-rich rocks from the Cloncurry district, NW Queensland, Australia: Lithos, v. 51, p. 223–245.

Mark, G., Darvall, M., Tolman, J., Foster, D.R.W., Williams, P.J., and Pollard, P.J., 1999, Magmas and regional Na-Ca alteration, Cloncurry district, Australia, *in* Stanley, C.J. et al., eds., Mineral deposits: Processes to processing: Rotterdam, Balkema, p. 385–388.

Mark, G., Oliver, N.H.S., Williams, P.J., Valenta, R.K., and Crookes, R.A., 2000, The evolution of the Ernest Henry hydrothermal system, *in* Porter, T.M., ed., Hydrothermal iron oxide copper-gold and related deposits: A global perspective: Adelaide, Australian Mineral Foundation, p. 132–136.

Marschik, R., and Fontboté, L., 2001, The Candelaria-Punta del Cobre iron oxide Cu-Au(-Zn-Ag) deposits, Chile: Economic Geology, v. 96, p. 1799–1826.

Marschik, R., Chiaradia, M., and Fontboté, L., 2003, Implications of Pb isotope signatures or rocks and iron oxide Cu-Au ores in the Candelaria-Punta del Cobre district, Chile: Mineralium Deposita, v. 38, p. 900–912.

Marshall, L.J., 2003, Brecciation within the Mary Kathleen Group of the Eastern Succession, Mount Isa block, Australia: Implications for Fe-oxide-Cu-Au mineralization: Unpublished Ph.D. thesis, Townsville, James Cook University of North Queensland, 325 p.

Marshall, L.J., and Oliver, N.H.S., 2002, From source to sink: Evolving fluid characteristics in Mount Isa inlier Fe-oxide-Cu-Au mineralization [abs]: Geological Society of Australia Abstracts, v. 67, p. 292.

McCrae, J.M., 1950, On the isotope chemistry of carbonates and a paleotemperature scale: Journal of Chemical Physics, v. 18, p. 849–857.

Oliver, N.H.S., 1995, The hydrothermal history of the Mary Kathleen fold belt, Mount Isa block, Queensland, Australia: Australian Journal of Earth Sciences, v. 42, p. 267–280.

Oliver, N.H.S., Valenta, R.K., and Wall, V.J., 1990, The effect of heterogeneous stress and strain on metamorphic fluid flow, Mary Kathleen, Australia, and a model for large-scale fluid circulation: Journal of Metamorphic Geology, v. 8, p. 311–331.

Oliver, N.H.S., Holcombe, R.J., Hill, E.J., and Pearson, P.J., 1991, Tectonometamorphic evolution of the Mary Kathleen fold belt, northwest Queensland: A reflection of mantle plume processes?: Australian Journal of Earth Sciences, v. 38, p. 425–455.

Oliver, N.H.S., Wall, V.J. and Cartwright, I., 1992, Internal control of fluid compositions in amphibolite-facies scapolitic calc-silicates, Mary Kathleen, Australia: Contributions to Mineralogy and Petrology, v. 111, p. 94–112.

Oliver, N.H.S., Cartwright, I., Wall, V.J., and Golding, S.D., 1993, The stable isotopic signature of large-scale fracture-hosted metamorphic fluid pathways, Mary Kathleen, Australia: Journal of Metamorphic Geology, v. 11, p. 705–720.

Oliver, N.H.S., Rawling, T.R., Cartwright, I., and Pearson, P.J., 1994, High temperature fluid-rock interaction and scapolitization in a large extension-related hydrothermal system, Mary Kathleen, Australia: Journal of Petrology, v. 35, p. 1455–1491.

Oreskes, N., and Einaudi, M.T., 1992, Origin of hydrothermal fluids at Olympic Dam: Preliminary results from fluid inclusions and stable isotopes: Economic Geology, v. 87, p. 64–90.

Page, R.W., 1983, Chronology of magmatism, skarn formation, and uranium mineralization, Mary Kathleen, Queensland, Australia: Economic Geology, v. 78, p. 838–853.

Page, R.W., and Sun, S-S., 1998, Aspects of geochronology and crustal evolution in the Eastern fold belt, Mount Isa inlier: Australian Journal of Earth Sciences, v. 45, p. 343–362.

Perkins, C., and Wyborn, L.A.I., 1998, Age of Cu-Au mineralization, Cloncurry district, Mount Isa inlier, as determined by $^{40}Ar/^{39}Ar$ dating: Australian Journal of Earth Sciences, v. 45, p. 233–246.

Perring, C.S., Pollard, P.J., Dong, G., Nunn, A.J., and Blake, K.L., 2000, The Lightning Creek sill complex, Cloncurry district, northwest Queensland: A source of fluids for Fe oxide-Cu-Au mineralization and sodic-calcic alteration: Economic Geology, v. 95, p. 1067–1089.

Pidgeon, R.T., Bosch, D., and Bruguier, O., 1996, Inherited zircon and titanite U-Pb systems in an Archaean syenite from southwestern Australia: Implications for U-Pb stability of titanite: Earth and Planetary Science Letters, v. 141, p. 187–198.

Pokrovskii, V.A., Harrold, B.P., Heinrich, C.A., and Liu, X., 1998, Release notes for THERMODATA AGSO/ANU/ETHZ (version 5.2) computer file: ETH (for availability contact C. Heinrich, Department Erdwissenschaften NO, ETH Zentrum, CH-8092 Zurich, Switzerland).

Pollard, P.J., 2001, Sodic(-calcic) alteration associated with Fe-oxide-Cu-Au deposits: An origin via unmixing of magmatic-derived H_2O-CO_2-salt fluids: Mineralium Deposita, v. 36, p. 93–100.

Pollard, P.J., Mark, G., and Mitchell, L.C., 1998, Geochemistry of post-1540 Ma granites in the Cloncurry district, northwest Queensland: Economic Geology, v. 93, p. 1330–1344.

Powell, R., 1977, Activity-composition relation for crystalline solutions, *in* Fraser, D.G., ed., Thermodynamics in geology: Dordrecht, D. Reidel, p. 57–65.

Reed, M.H., and Spycher, N.F., 1985, Boiling, cooling, and oxidation in epithermal systems: A numerical approach: Reviews in Economic Geology, v. 2, p. 249–272.

Rose, N.M., Bird, D.K., and Liou, J.G., 1992, Experimental investigation of mass transfer—albite, Ca Al silicates and aqueous solutions: American Journal of Science, v. 292, p. 21–57.

Rotherham, J.F., Blake, K.L., Cartwright, I., and Williams, P.J., 1998, Stable isotope evidence for the origin of the Starra Au-Cu deposit, Cloncurry district: Economic Geology, v. 93, p. 1435–1449.

Rubenach, M.J., and Barker, A.J., 1998, Metamorphic and metasomatic evolution of the Snake Creek anticline, Eastern Succession, Mount Isa inlier: Australian Journal of Earth Sciences, v. 45, p. 363–372.

Rubenach, M.J., and Lewthwaite, K.J., 2002, Metasomatic albitites and related biotite-rich schists from a low-pressure polymetamorphic terrane, Snake Creek anticline, Mount Isa inlier, northeastern Australia: Microstructures and P-T-d paths: Journal of Metamorphic Geology, v. 20, p. 191–202.

Rubenach, M.J., Adshead, N.D., Oliver, N.H.S., Tullemans, F., Esser, D., and Stein, H., 2001, The Osborne Ca-Au deposit: Geochronology and genesis of mineralization in relation to host albitites and ironstones [ext. abs.]: Townsville, Australia, James Cook University, School of Earth Sciences, Economic Geology Research Unit Contribution, v. 59, p. 172–173.

Rumble, D., III, 1982, Stable isotope fractionation during metamorphic devolatilization reactions: Reviews in Mineralogy, v. 10, p. 327–353.

Scott, D.J., and St-Onge, M.R., 1995, Constraints on Pb closure temperature in titanite based on rocks from the Ungava orogen, Canada: Implications for U-Pb geochronology and P-T-t path determinations: Geology, v. 23, p. 1123–1126.

Sharp, Z.D., and Kirschner, D.L., 1994, Quartz-calcite oxygen isotope thermometry: A calibration based on natural isotopic variations: Geochimica et Cosmochimica Acta, v. 58, p. 4491–4501.

Shock, E.L., Sassani, D.C., Willis, M., and Sverjensky, D.A., 1997, Inorganic species in geologic fluids: Correlations among standard molal thermodynamic properties of aqueous ions and hydroxide complexes: Geochimica et Cosmochimica Acta, v. 61, p. 907–950.

Shvarov, Y.V., 1978, Minimization of the thermodynamic potential of an open chemical system: Geochemistry International, v. 15, p. 38–45.

——1999, Algorithmization of the numerical equilibrium modeling of dynamic geochemical processes: Geochemistry International, v. 37, p. 571–576.

Shvarov, Y.V., and Bastrakov, E.N., 1999, HCh: A software package for geochemical equilibrium modeling, user's guide: Australian Geological Survey Organisation Record 1999/25, 60 p.

Sillitoe, R.H., 2003, Iron oxide-copper-gold deposits: An Andean view: Mineralium Deposita, v. 38, p. 787–812.

Skirrow, R.G., and Walshe, J.L., 2002. Reduced and oxidized Au-Cu-Bi iron oxide deposits of the Tennant Creek inlier, Australia: An intregrated geologic and chemical model: Economic Geology, v. 97, p. 1167–1202.

Sverjensky, D.A., Hemley, J.J., and D'Angelo, W.M.D., 1991, Thermodynamic assessment of hydrothermal alkali feldspar-mica-aluminosilicate equilibria: Geochimica et Cosmochimica Acta, v. 55, p. 989–1004.

Sverjensky, D.A., Shock, E.L., and Helgeson, H.C., 1997, Prediction of the thermodynamic properties of aqueous metal complexes to 1000°C and 5 kb: Geochimica et Cosmochimica Acta, v. 61, p. 1359–1412.

Twyerould, S.C. 1997, The geology and genesis of the Ernest Henry Fe-Cu-Au deposit, Northwest Queensland, Australia: Unpublished Ph.D. thesis, Eugene, Oregon, University of Oregon, 494 p.

Ulrich, T., and Heinrich, C.A., 2001, Geology and alteration geochemistry of the porphyry Cu-Au deposit at Bajo de la Alumbrera, Argentina: Economic Geology, v. 96, p. 1719–1742.

Valley, J.W. 1986, Stable isotope geochemistry of metamorphic rocks: Reviews in Mineralogy, v. 16, p. 445–490.

Vanko, D.A., and Bishop, F.C., 1982, Occurrence and origin of marialitic scapolite in the Humboldt lopolith, N.W. Nevada: Contributions to Mineralogy and Petrology, v. 81, p. 277–289.

Wickham, S.M., and Taylor, H.P., Jr., 1987, Stable isotope constraints on the origin and depth of penetration of hydrothermal fluids associated with Hercynian regional metamorphism and crustal anatexis in the Pyrenees: Contributions to Mineralogy and Petrology, v. 95, p. 255–268.

Williams, P.J., 1994, Iron mobility during synmetamorphic alteration in the Selwyn Range area, NW Queensland: Implications for the origin of ironstone-hosted Au-Cu deposits: Mineralium Deposita, v. 29, p. 250–260.

——1998, Metalliferous economic geology of the Mount Isa Eastern Succession, Queensland: Australian Journal of Earth Sciences, v. 45, p. 329–341.

Williams, P.J., Dong, G., Pollard, P.J., Perring, C.S., Ryan, C.G., and Mernagh, T.P., 1999, Fluid inclusion geochemistry of Cloncurry (Fe)-Cu-Au deposits, *in* Stanley, C.J., ed., Mineral deposits: Processes to processing: Rotterdam, Balkema, p. 111–114.

Williams, P.J., Dong, G., Ryan, C.G., Pollard, P.J., Rotherham, J.F., Mernagh, T.P., and Chapman, L.H., 2001, Geochemistry of hypersaline fluid inclusions from the Starra (Fe oxide) Au-Cu deposit, Cloncurry district, Queensland: Economic Geology, v. 96, p. 875–884.